Author(s): Mahajan, Shreya; Elfving, Jere; Lahtinen, Manu

Title: Evaluating the viability of ethylenediamine-functionalized Mg-MOF-74 in direct air
capture : The challenges of stability and slow adsorption rate

Year: 2024

Version: Published version

Evaluating the viability of ethylenediamine-functionalized Mg-MOF-74 in direct air capture: The challenges of stability and slow adsorption rate

Shreya Mahajan [a], Jere Elfving [b], Manu Lahtinen [a],[*]

[a] *Department of Chemistry, University of Jyväskylä, P.O. Box 35, FI-40014 Jyväskylä, Finland*
[b] *VTT Technical Research Centre of Finland Ltd., Koivurannantie 1, FI-40101 Jyväskylä, Finland*

ARTICLE INFO

ABSTRACT

Carbon removal technologies, such as direct air capture (DAC), hold great potential in mitigating anthropogenic CO_2 emissions. Amine-tethered metal-organic frameworks (MOFs) that capture CO_2 selectively *via* chemisorption have been highlighted as frontrunners for CO_2 removal technologies. To this end, ethylenediamine (ED) was employed to decorate the metal sites of Mg-MOF-74, and both bare and amine-modified frameworks were thoroughly characterized and studied for DAC using an automated fixed-bed sorption device. The material exhibited a promising CO_2 capacity of up to 1.8 mmol/g from 400 ppmv CO_2 in humid conditions, although the amount of adsorbed H_2O was several times higher. The highest adsorption capacities were measured at 25–35 °C, while decreased capacity was observed at 12 °C due to slower adsorption rate. In dry cyclic adsorption-desorption tests, the cyclic CO_2 capacity reduced slightly in 18 cycles. However, at 2 vol% humidity, the capacity dropped rapidly over successive cycles, revealing poor hydrolytic stability. Preliminary coating experiments were conducted on stainless steel plates and cordierite monoliths, suggesting that reasonably even coating layers could be achieved on these substrates with relatively simple coating techniques. High water adsorption, slow adsorption rate at low temperatures, and the rapid cyclic capacity decrease in humid conditions may limit the application of the studied adsorbent for DAC. The vital aspects of the real application of MOFs in DAC, such as adsorption kinetics and stability in humid conditions, are rarely explored in detail in the literature, and these results indicate that these aspects warrant extensive study for the development of practically applicable DAC adsorbents.

1. Introduction

The average global temperature has already risen by 1 °C (relative to pre-industrial levels), and it is projected to reach 1.5 °C within the next decade, amplifying the risk of surpassing 2 °C. The approach to limiting the temperature rise is to reduce emissions while, in parallel, implementing the negative emissions on a multi-Gt/y scale of CO_2. These negative emission technologies (NETs) [1] accelerate the removal of already released CO_2 and come in various types, for example, biochar (BC), afforestation and reforestation (AR), bioenergy with carbon capture and storage (BECCS), and direct air capture (DAC) in conjunction with carbon storage, to name a few [2]. Three of these NETs employ photosynthesis to capture CO_2 from the air, while DAC extracts atmospheric CO_2 using physicochemical processes (including solvents or solid adsorbents) [3,4]. Of all the NETs, DAC is particularly advantageous due to its smaller land requirement and significantly lower water usage, [5] albeit it still needs further technological development to be fully realized [6].

In direct air capture, atmospheric air is typically blown through a contactor containing the CO_2-capturing material until the desired saturation is achieved. After the capture step, the CO_2-capturing material is regenerated, typically with heat, to produce high-concentration CO_2, which can be compressed, reliably stored, or utilized [7–9]. Among an array of CO_2-capturing materials, a high volume of research has been conducted on amine-modified porous solids, which are made by combining amines with support materials such as silica, carbon, alumina, and porous polymers [10–14]. In principle, these adsorbents are highly recognized for their relatively enhanced adsorption and favorable single-gas selectivity among other CO_2-capturing materials, even at low concentrations and in the presence of moisture. Compared to solvent-based DAC [7], using amine-adsorbents enables a relatively simple temperature-vacuum swing adsorption (TVSA) DAC process

where the adsorbent can be regenerated only at around 80–100 °C [8,9].

Unfortunately, amine-functionalized sorbents often incur severe challenges that hamper their applicability for DAC. These can be related to CO_2 capacity, adsorption/desorption kinetics, regenerability, and cyclic stability under varying atmospheric conditions. A combination of sub-optimal parameters or one undesirable characteristic, such as fast degradation over repeated adsorption/desorption cycles [15], can render a CO_2 sorbent practically useless for CO_2 capture from air. Despite the drawbacks mentioned above, amine-based solid materials have been identified as a vital component in DAC technology. The supported molecular amines possess the ability to chemisorb low-concentration CO_2 from the atmospheric air, resulting in enhanced adsorption. Therefore, the prominent role of amines makes them a significant area of focus for atmospheric CO_2 capture.

Advanced porous hybrid materials called Metal-organic frameworks (MOFs) [10,16–19] are an emerging material group that holds tremendous promise in surmounting these challenges and have been highlighted as frontrunners for CO_2 capture technologies. Among the library of MOFs explored, the MOFs repleted with unsaturated or open metal sites (OMSs) on the surfaces of the pores have been revealed to be outstanding for gas adsorption and separation [18,19]. For instance, the pore size (~11 Å) and high density of OMSs within evacuated Mg-MOF-74 ($Mg_2(dobdc)$, H_4dobdc = 2,5-dioxidobenzene-1,4-dicarboxylic acid; CPO-27-Mg) [20–24] lined along its 1D channels have enabled them to be exceedingly examined for CO_2 adsorption. Therefore, Mg-MOF-74 is one of the best-studied adsorbents for higher concentrations of CO_2 (10–15%) relevant to post-combustion capture [21]. Previous studies on M-dobdc series (M stands for a metal center, *i.e.*, M = Mg^{2+}, Ni^{2+}, Co^{2+}, Zn^{2+}) have demonstrated that these exposed metal cations engage strongly with incoming CO_2 because of its greater polarizability (29.1 × 10^{-25} cm^{-3}) and quadrupole moment (13.4 × 10^{-40} C·m²) [17,25]. However, the Mg-MOF-74 is considerably sensitive toward moisture owing to the tendency of H_2O to out-compete CO_2 [26]. As a result, the structure experiences a reduction in reactive sites [27,28], which has been measured to result in only 16% of the initial capacity after regeneration for post-combustion capture under 70% relative humidity [29]. Seemingly, chemical instability under humid conditions and low CO_2 selectivity obviates its applicability in realistic DAC operations [19].

An important point to note is that the adsorbents desirable for flue gas CO_2 capture are not primed to excel in DAC because of the lower concentration of CO_2 in the air (~0.04%) as opposed to flue gas (~5–15%). For that reason, an adsorbent with reasonably strong binding to CO_2 is required to attain an appreciable amount of gas uptake but not so strong as to impede the regeneration process [30]. Taking advantage of MOFs with exposed metal cations, they can be modified through post-synthetic functionalization by introducing diamine groups into their pores. For example, in Mg-MOF-74, attaching one amine of the diamine directly to the Mg^{2+} and utilizing terminal amine (free Lewis's base) as a CO_2 adsorptive site to selectively capture CO_2 *via* chemisorption.

In a study by Choi et al. [31], Mg-MOF-74 was functionalized with ethylenediamine (ED) to capture CO_2 from dry simulated air (400 ppm CO_2/Ar) on a TGA. The aminated-MOF adsorbed 1.51 $mmol_{CO2}/g_{sorbent}$, around a 12% enhancement to its pristine MOF. To investigate the regenerability of the adsorbents, a 4-cycle adsorption-desorption experiment was conducted following temperature-swing adsorption (TSA), where the parent MOF experienced a 20% drop in its initial CO_2 uptake (1.35 to 1.06 $mmol_{CO2}/g_{sorbent}$). At the same time, aminated-MOF maintained its capacity without any decline. In a follow-up study, both ED-grafted $Mg_2(dobdc)$ and bare $Mg_2(dobdc)$ were subjected to steam treatment (110 °C in steam/N_2, 48 h) utilizing an autoclave reactor [32]. The TGA adsorption experiment (pure CO_2 at 25 ºC) showed a negligible loss in CO_2 capacity for the aminated-MOF (4.66 to 4.47 $mmol_{CO2}/g_{sorbent}$), while bare $Mg_2(dobdc)$ experienced a 60% loss, dropping from 4.27 to 1.71 $mmol_{CO2}/g_{sorbent}$. To date, no studies have been conducted on the co-adsorption of CO_2 and H_2O in ED-grafted $Mg_2(dobdc)$, nor has there been any research on its ability to undergo extended adsorption-desorption cycles under a humid DAC environment. In fact, the kinetics of CO_2 adsorption under DAC conditions remain understudied. Indeed, it is reasonable to say that the lack of this valuable data limits the feasibility of this material for dilute streams.

Thus, to facilitate the deployment of DAC at the global level, it is pivotal to investigate and understand how CO_2 sorbent materials perform under realistic working conditions. For example, the temperature at which adsorption occurs is crucial in DAC research [19]. Since the realistic DAC systems operate in different climatic environments with a relatively broad temperature range (−30 to 50 °C), testing the adsorbent's performance under a range of operating conditions, not just at room temperature (25 °C), is necessary [30,33]. In addition to temperature, moisture in the air is another benchmark parameter that can drastically impact CO_2 capacity and influence the overall operation of the DAC process. For example, an investigation was conducted to determine the impact of humidity on the performance of the M-dobdc series using a gas-flow apparatus under conditions that are pertinent to post-combustion capture [29]. After regeneration from hydration at 70% RH, it was discovered that $Co_2(dobdc)$, $Ni_2(dobdc)$, and $Mg_2(dobdc)$ experienced a reduction in CO_2 capacity of 15%, 40%, and 84%, respectively [29,30]. In a separate study, Adil et al. [34] demonstrated that the mmen-$Mg_2(dobpdc)$ had a high breakthrough time after exposure to dry mixed-gas adsorption (CO_2/N_2:10/90 mixture) conditions. However, its performance was compromised immensely over the course of 5 humid cycles, noticeable by a 30% drop in CO_2 retention time. Although the data reported corresponds to mostly studying flue gas, the results imply the need for focused studies on CO_2/H_2O competitive adsorption at realistic dilute CO_2 concentrations [30].

Additionally, when assessing MOFs for the DAC potential, it is essential to consider that sorbent stability is just as crucial as the adsorption temperature and humidity. It is a particularly key parameter because any economically viable DAC adsorbent should withstand thousands of adsorption-desorption cycles without exhibiting performance decay [15]. Eventually, the degradation of amine-based adsorbents may be a crucial bottleneck for the application of DAC in the required Gt-scale, as well as from an environmental point-of-view, if left unsolved [1]. Besides, prior to industrial utilization, it is necessary to formulate amine-based powdered adsorbents into larger pellets or apply the adsorbent as a coating on different substrates to prevent intrinsic hurdles with processing, *e.g.*, handling, pressure drops, and fluidization of the MOF particles [35–37].

On these described key aspects, the work aims to assess the performance of ED-functionalized $Mg_2(dobdc)$ (hereafter ED@MOF-74) in both dry and humid DAC-relevant conditions using a fixed-bed adsorption setup, which has never been systematically studied to the best of our knowledge. In this study, both nonfunctionalized Mg-MOF-74 and amine-modified framework were thoroughly characterized using Powder X-ray diffraction (PXRD), thermogravimetric analysis (TGA), Fourier transform infrared spectroscopy (FT-IR), scanning electron microscopy (SEM), and Elemental analyses (EA). Herein, we report the first detailed study of ED@MOF-74 in temperature-concentration swing adsorption (TCSA) mode and provide insight into how varying operating conditions, such as temperature, adsorption time and humidity, impact CO_2 adsorption. Finally, we performed cyclic experiments under both dry and humid conditions. The samples were fully evaluated post-cycling experiment using PXRD, FT-IR, and EA. We deliberately selected ED@MOF-74 because its long-term use for carbon capture is unknown. Notably, we also explored the coating of the ED@MOF-74 on stainless steel plates and cordierite monoliths, the preliminary results of which are included in this article.

2. Syntheses and methods

All the reagents and solvents were purchased from standard

commercial sources and utilized as received unless otherwise stated.

2.1. Syntheses

2.1.1. Synthesis of Mg-MOF-74

The synthesis of Mg-MOF-74 was performed successfully on a gram scale at room temperature following the reported method with slight modification [38]. $Mg(NO_3)_2 \cdot 6H_2O$ [5.18 g, 20.19 mmol] and linker 2, 5-dihydroxyterephthalic acid (H_4dobdc) [2.00 g, 10.09 mmol] were dissolved separately in methanol (MeOH) [49.7 mL], and an aqueous solution of sodium hydroxide [1 M, 40 mL, 40 mmol] respectively. Subsequently, the clear linker solution was slowly added to the magnesium salt solution with continuous stirring at room temperature. After 24 h, the precipitate was isolated *via* filtration, then thoroughly washed with MeOH [3 × 50 mL] and deionized water [5 × 100 mL]. Finally, it was dried overnight at 150 ºC in *vacuo*, resulting in a yellow solid (Yield: 64.1%). Anal. Calc. for $C_8H_9Mg_2O_{9.5}$: C, 31.43; H, 2.97. Found: C, 31.75; H, 3.18%. FT-IR (cm^{-1}): 3341, 2188, 1585, 1423, 1371, 1235, 1215, 1120, 1022, 888, 819, 583, 488.

2.1.2. Synthesis of ED@MOF-74

Prior to amine functionalization, 1 g of Mg-MOF-74 was loaded in a two-neck round-bottom flask and activated under high *vacuo* at 200 ºC for 2 h and then reacted with ethylenediamine (ED) [~4 g] in anhydrous toluene [100 mL] *via* extensive refluxing under inert atmosphere for 24 h. The dark yellowish powder was collected by filtration, rinsed with copious amounts of toluene and hexane, and dried at 120 ºC in *vacuo* for 4 h (Yield: 89.5%). Anal. Calc. for $C_{11.6}H_{21.8}N_{3.6}Mg_2O_{8.7}$: C, 34.87; H, 5.50; N, 12.62. Found: C, 35.15; H, 5.06; N, 13.11%. FT-IR (cm^{-1}): 3352, 3290, 2943, 2868, 1574, 1453, 1415, 1370, 1212, 1114, 967, 911, 884, 817, 639, 579, 480, 406. The comparison of the FT-IR spectra (cm^{-1}) is illustrated in Fig. 3.

2.2. Characterization of the MOFs

2.2.1. Powder X-ray diffraction (PXRD)

PXRD data were measured using a Panalytical X'Pert PRO diffractometer with Cu K_α radiation ($\lambda = 1.54187$ Å; Ni β-filter; 45 kV, 40 mA). Each powder sample was attached to a silicon-made "zero-background signal generating" plate using petrolatum jelly as an adhesive. Diffraction intensities were recorded by an X'Celerator detector at room temperature with 2θ-range of 3–60°, a step size of 0.017°, and a counting time of 70 s per step. Data processing, search-match phase analyses and the Pawley fits were carried out by the program X´pert HighScore Plus (v. 4.9). Search-match phase identification analyses were made against the ICDD-PDF4 + database (version 2022) implemented in the HighScore [39,40]. In the Pawley fit, the refined parameters were zero-offset, polynomial background, sample height displacement, unit cell parameters, and peak profile parameters (peak width, shape, and asymmetry).

2.2.2. Thermal analysis

The thermal properties of the materials have been analyzed using a Perkin Elmer STA 6000 simultaneous thermogravimetric/calorimetric (TG/DSC) analyzer. Each sample was prepared in an open platinum pan and heated under N_2 (flow rate of 40 mL/min) with a heating rate of 10 °C/min in a temperature range of 22–600 °C. Temperature calibration of the analyzer was made using melting points of the indium (156.6 °C), zinc (419.5 °C), and aluminum (660.3 °C) standards. The weight balance was calibrated at room temperature using a standard weight of 50.00 mg. The sample weights used in the measurements were about 5–10 mg.

2.2.3. Other methods

The morphology analysis of the samples was performed using Zeiss EVO-50XVP scanning electron microscopy (SEM). The Fourier transform infrared (FT-IR) spectra were recorded using Bruker Alpha II ATR instrument over a 4000–400 cm^{-1} range with 2 cm^{-1} spectral resolution. Prior to pressing a small amount of a sample onto the diamond ATR Prism, the sample was mildly ground, and the spectrum obtained was baseline corrected. Elemental analyses (C, H, and N) were conducted in-house using an Elementar EL III analyzer.

2.3. Fixed-bed DAC experiments

An automated fixed-bed adsorption/desorption device was used to investigate the applicability of the ED@MOF-74 for CO_2 adsorption from air. Examples of this device include the adsorption of CO_2 from ultra-dilute concentrations in dry and humid conditions [41], cyclic adsorption/desorption experiments, and a comparison of different desorption methods [42]. The device's instrumentation, operation, scheme of the setup and other details can be found in [42,43]. Approximately 0.1 g of the studied MOF was loaded into the adsorption column. With the measured bulk density of 0.4 g/mL, the length of the adsorbent bed is thus around 0.4 cm. Therefore, the temperature sensor inside the column was around 0.6 cm above the sample, measuring the temperature of the adsorption column rather than the sample bed. Approximately 0.15 g of quartz wool was inserted above the sample to prevent the downstream loss of the small MOF particles.

The CO_2 adsorption runs were based on the temperature-concentration swing adsorption (TCSA) scheme. The sample was typically regenerated at 120 °C under nitrogen flow for several hours until no CO_2 was detected in the outlet, then cooled down to the adsorption temperature. Adsorption was conducted using dry or humidified feed with around 400 ppmv CO_2 using 1% CO_2/N_2, with purities of 3.5 CO_2 and 5.0 N_2, balanced with 5.0 N_2. After the adsorption step, the purge step was initiated by switching the CO_2-containing feed to pure nitrogen, and the total desorption was achieved by heating the sample again to the regeneration temperature under nitrogen flow. The total flow rate was kept at 200 mL/min during adsorption and desorption. All breakthrough experiments were run at approximately 1 bar total pressure.

One experiment was conducted on Mg-MOF-74 using the temperature-vacuum-concentration swing adsorption (TVCSA) scheme. This experiment differed from the TCSA scheme by incorporating vacuuming in addition to purge and temperature swing steps. During the vacuuming step, the feed N_2 flow rate remained constant at 100 mL/min, and the column pressure was decreased in a stepwise manner by opening the pressure control valve in small increments.

Adsorption-desorption experiments with the ED@MOF-74 were conducted using variable temperature, adsorption time, and humidity conditions. These conditions and the measured capacity results are found in Section 3.2 below. In cyclic stability tests (Section 3.3), the adsorption time was 5 h, and the adsorption temperature was 25 °C. Otherwise, all these experiments followed the TCSA scheme as described above. Two different experiments were conducted to study the effect of adsorption temperature on CO_2 capacity. In the first one, a constant feed of around 400 ppmv CO_2 was used, and the temperature was increased in a stepwise fashion. The Supporting Information describes these results and the method in more detail. The second experiment was conducted using a similar scheme for the cyclic stability tests, except that the 12-hour adsorption step varied in adsorption temperature. To differentiate it from the shorter cyclic stability tests, this experiment is referred to as the "long cyclic" experiment in the text, and the results are presented in Section 3.2.1.

The adsorption and desorption capacities were calculated by numerical integration ("cumtrapz"-function in Matlab) of the adsorption/desorption profile and using ideal gas law, as described in more detail in [43]. The feed was typically measured from the outlet when bypassing the column before the adsorption step was begun, like in earlier work [41–43]. However, due to the low flow rate, in some cases, the feed CO_2 concentration was not stabilized during the time that the feed was directed through the bypass. In these cases, the feed was either measured at the end of the adsorption step or separately after the

desorption. On the other hand, in the case of H_2O, the feed was measured from the end of adsorption or from the highest concentration value during adsorption in most cases. This way, the mass balance between adsorption and desorption of H_2O was better maintained compared to measuring the feed from the bypass. The effect of the feed concentration and challenges related to measuring the feed and experimental uncertainty are discussed in more detail in the Supporting Information.

## 3. Results & discussion

3.1. Structural characterization

The crystallinity and phase purity of the materials were corroborated *via* Powder X-ray diffraction (PXRD). The Pawley refinement was facilitated using the Xpert HighScore Plus program to verify the phase purity of the synthesized pristine MOF (Fig. 1). The Pawley refinement of the unit cell parameters for the powdered material prepared at room temperature (24 h) was structurally equivalent to the single crystal structure of CPO-27-Mg reported by Dietzel et *al.* [23] (Table S1). The two prominent Bragg diffraction peaks, [31] at $2\theta = 6.8$ and 11.8, confirmed the successful bulk synthesis of Mg-MOF-74 without any phase impurity peaks detected.

The PXRD results also revealed that the framework integrity remained intact following the ED grafting procedure, with only slight shifts in peak positions and a few relatively lowered peak intensities (Fig. 2).

The Fourier transform infrared spectroscopy (FT-IR) measurement was further conducted to establish the successful synthesis of Mg-MOF-74 and confirm the presence of amine sites in ED@MOF-74. The spectral changes occurring in both materials are visualized in Fig. 3. First, by comparing the IR spectrum of the 2,5-dihydroxyterephthalic acid ligand (H_4dobdc) with pristine MOF, it was observed that the characteristic peak at ~1640 cm^{-1} attributed to the free carboxylic acid group was present in the linker but vanished in Mg-MOF-74. Instead, new bands

associated with $\nu_{as}(COO^-)$ and $\nu_s(COO^-)$ modes developed and are recorded at ~1585 and 1371 cm^{-1}, respectively, demonstrating the successful carboxylate coordination to the Mg^{2+} sites. In addition, the characteristic band corresponding to the phenolic group stretch $\nu(C–O)$ is centered at ~1235 cm^{-1} [44] (Fig. 3a). Thus, on this basis, both carboxylic and hydroxyls were practically identified to be deprotonated during the room temperature synthesis. Further, with the introduction of ED, new spectral features emerged related to amine modes, and the spectral bands associated with the linker experienced a tiny shift. Noticeably, in ED@MOF-74, bands associated with $\nu_{as}(COO^-)$ and $\nu_s(COO^-)$ modes are slightly shifted to ~1574 and 1370 cm^{-1}, respectively. The new principal bands detected in ~3352–3290 and ~2943–2868 cm^{-1} are ascribed to N–H and aliphatic C–H bond stretching modes, respectively (Zoomed-in data, Fig. 3b). In addition, the deformation mode of CH_2 and aliphatic C–C stretching are observed around 1453 and 967 cm^{-1}, respectively, highlighting the successful incorporation of ED [44,45].

The ED content was further quantified through thermogravimetric analyses conducted at 10 °C/min under a nitrogen flow. Fig. 4a compares the thermograms of Mg-MOF-74 and ED@MOF-74, with results tabulated in Table S2. As can be seen in Fig. 4, the Mg-MOF-74 displays a gentle descending two-step decomposition route, wherein a first region, the weight loss of 20.02 wt.-% (calcd. 20.60%) up to 310 °C, is attributable to the release of occluded and coordinated water molecules, which is consistent with the previous literature [46]. The ED@MOF-74, on the other hand, demonstrated a weight loss of approximately 8.87 wt.-% (calcd. 9.01%) and 6.53 wt.-% (calcd. 7.52%) in two steps, which correlates to the loss of non-coordinated water and ED molecules in the temperature range of 23–124 °C and 124–218 °C, respectively. Further, the third mass decay of 21.67 wt.-% (calcd. 22.70%) between 218–440 °C resulted from the removal of metal-bound water and ED molecules, and finally, above 440 °C the weight loss was associated with the primary decomposition process. Thus, in accordance with the EA results of the studied ED@MOF-74 sample, the proposed formula $[Mg_2(dobdc)(H_2O)_{0.7}(ed)_{1.3}]\cdot 2\,H_2O\cdot 0.5(ed)$ is in close agreement as
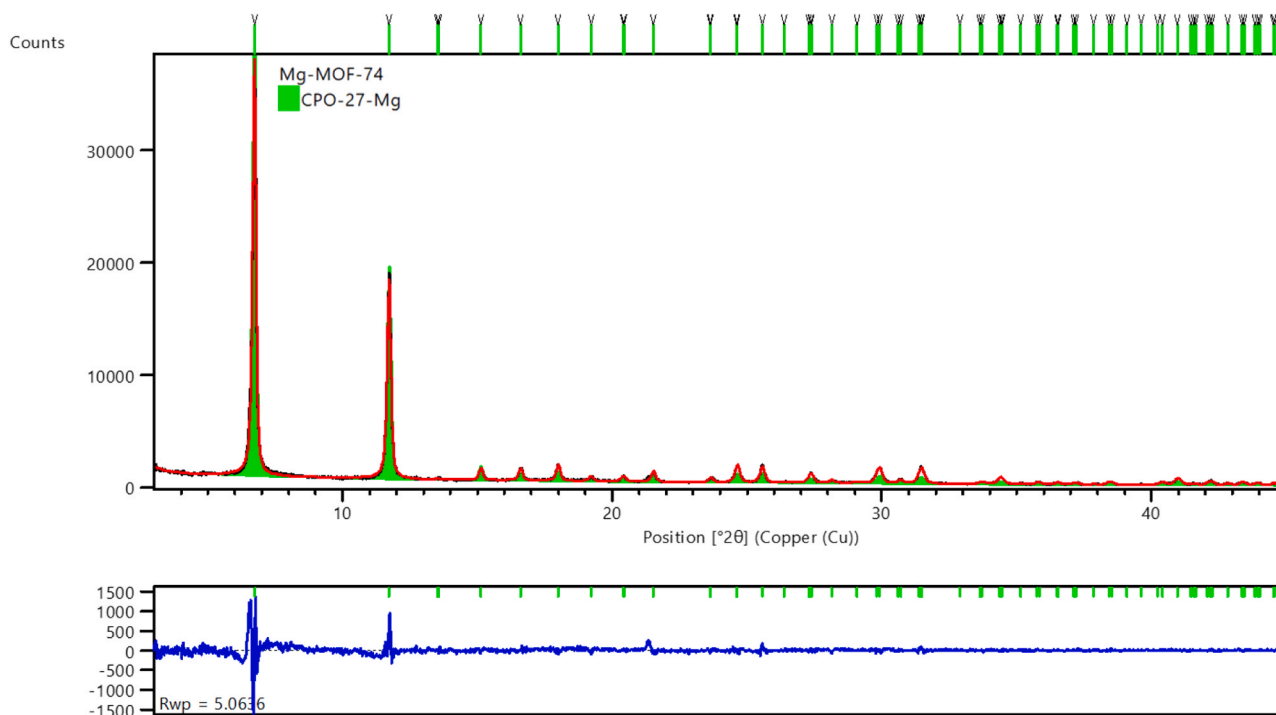
Fig. 1. Pawley refinement plot of Mg-MOF-74. The experimental pattern is black, and the refined profile is red. In contrast, green colored markers on top correspond to characteristic Bragg peak positions of the refined unit cell of the structure reported by Dietzel et *al.* [23] (CSD entry: MOHGOI). The difference plot of experimental *vs.* refined profiles is shown below in blue.
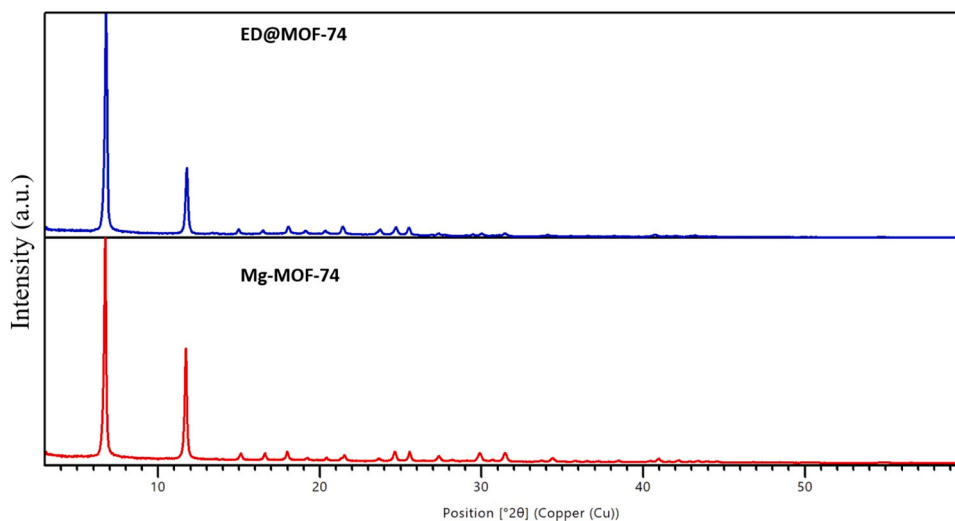
Fig. 2. Powder X-ray Diffraction Patterns of Mg-MOF-74 (red) and ED@MOF-74 (blue).

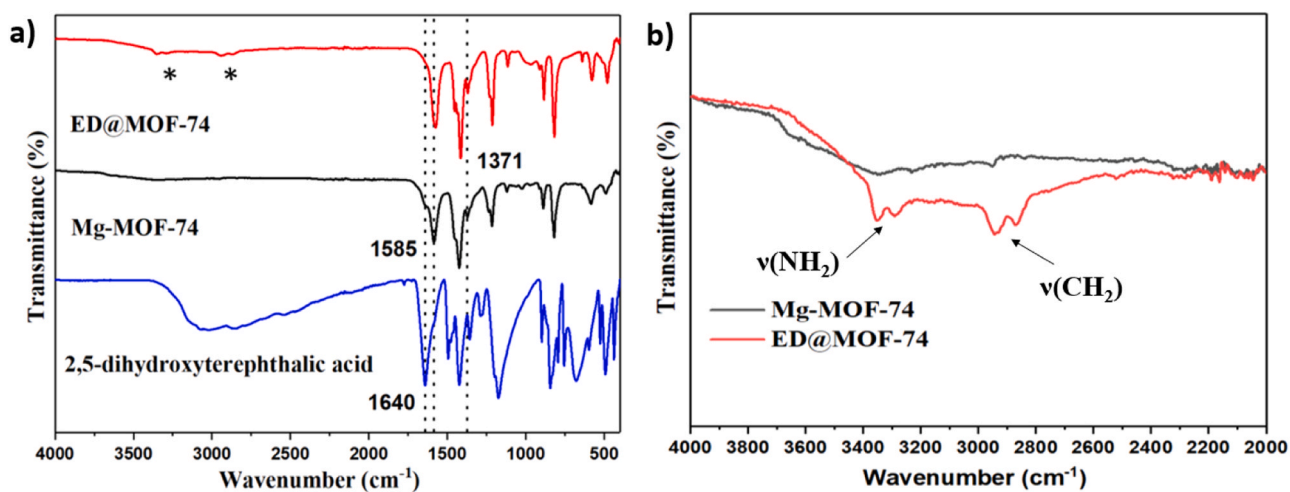**Fig. 3.** a) FT-IR (cm^{-1}) spectra of 2,5-dihydroxyterephthalic acid ligand (H$_4$dobdc, blue), Mg-MOF-74 (black), and ED@MOF-74 (red). b) Magnification of the bands marked with *(region of ED).
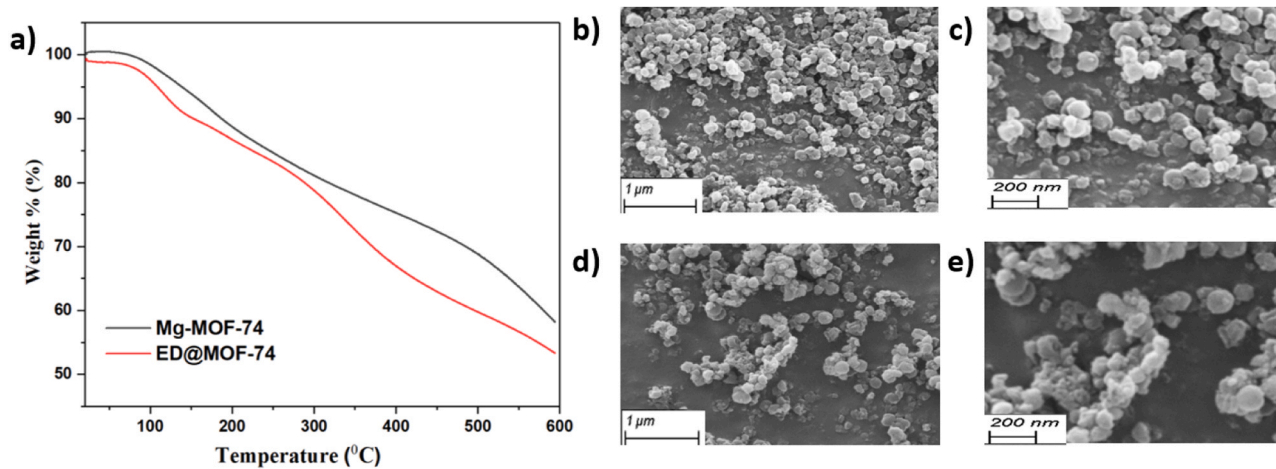

Fig. 4. a) TG curves of Mg-MOF-74 (black) and ED@MOF-74 (red), SEM images for b, c) Mg-MOF-74, and d, e) ED@MOF-74 at different magnifications.

supported by the thermogravimetric analysis.

Scanning Electron Microscopy (SEM) was performed to corroborate the morphology following the ED modification. SEM images for Mg-MOF-74 and ED@MOF-74 demonstrate that their morphology remained intact after functionalization (Fig. 4b-e). The particles have a softer, powdery texture resembling small conglomerates with a cotton-ball-like morphology, with an average size of about 300–400 nm [38].

3.2. CO_2 adsorption from air

A set of adsorption experiments was conducted in variable conditions to screen the performance of the MOFs in DAC conditions. The pristine Mg-MOF-74 was tested first using the TVCSA scheme, as described in Section 2.3. The adsorption capacity of the pristine MOF in the presence of 400 ppmv CO_2 at 25 °C was around 0.03 $mmol_{CO2}/g_{sorbent}$. Since the estimated minimum fluidization velocity was much exceeded in the studied conditions, vacuuming was not employed in the following runs to avoid the loss of adsorbent from the bed. In the first experiment with ED@MOF-74, the sample was regenerated at 100 °C, and adsorption was conducted in dry conditions for 12 h. The sample reached pseudo-equilibrium based on the outlet CO_2 concentration reaching the feed. The achieved CO_2 adsorption capacity was around 0.4 $mmol_{CO2}/g_{sorbent}$, imparting a significant enhancement in adsorption performance in DAC conditions compared to the unmodified MOF. A summary of the measured capacities in different experiments conducted in this study is shown in Table 1, while a more detailed table is available in the Supporting Information.

It is shown in Table 1 that the adsorption results are higher in most cases than the respective desorption capacities. Similar behavior has been observed earlier in the case of H_2O, while for CO_2, this difference has been relatively small, if any [41]. The main reason for this difference between adsorption and desorption capacities originates from the adsorption measurement method, as discussed in previous work [41, 47]. The measured feed's uncertainty significantly affects the calculated adsorption capacity, as shown in the Supporting Information. However, the differences between adsorption and desorption capacities fall within the experimental uncertainty, and the mass balance between the steps is well maintained.

In the following experiment, a higher regeneration temperature of 120 °C was used (100 °C in the first test) to achieve more complete regeneration, as it was suspected to be incomplete at 100 °C. The higher temperature was selected as the capacity resulting in the first experiment was deemed low in comparison to 1.5 $mmol_{CO2}/g_{sorbent}$ in dry DAC conditions reported by Choi et *al.* [31]. Consequently, the higher regeneration temperature increased the CO_2 capacity from approximately 0.4 $mmol_{CO2}/g_{sorbent}$ to 0.7 $mmol_{CO2}/g_{sorbent}$ and 0.8 $mmol_{CO2}/g_{sorbent}$ in adsorption and desorption, respectively. However, after three cycles in different conditions of humidity and adsorption temperature, the adsorption was measured again in dry conditions at 25 °C, resulting in an even higher adsorption capacity of 0.98 $mmol_{CO2}/g_{sorbent}$. A repeated cycle in similar adsorption conditions resulted in a slightly lower capacity of 0.90 $mmol_{CO2}/g_{sorbent}$, although the difference falls within experimental uncertainty. The increase in adsorption capacity from the second experiment done in similar conditions compared to the sixth and seventh experiments could be due to changes in the sample due to multiple repeats of adsorption and desorption. Another reason could be the introduction of humidity in the third and fourth experiments. Although the removal of H_2O was deemed complete after the humid cycles, as no humidity was detected in the outlet at the end of desorption, it is possible that humidity within the MOF structure enabled a complete regeneration when purging the sample with nitrogen at 120 °C. The effect of adsorption temperature and humidity on the adsorption of CO_2 is discussed in more detail below.

3.2.1. Effect of adsorption temperature

The adsorption of CO_2 on amine-functionalized materials is governed by adsorption equilibrium and mass transfer, which is why it is essential to study the rate of adsorption and the measured final adsorption uptakes at different temperatures. Fig. 5 shows the CO_2 adsorption breakthrough data on the ED@MOF-74 at different temperatures in the long cyclic experiment. The feed was reached earlier at higher temperatures, which could be attributed to both lower adsorption capacity and increased kinetics at higher temperatures. For example, at 77 °C and 102 °C, the CO_2 concentration sharply increases towards the feed already at the start of the experiment. On the other hand, the CO_2 concentration increases slower towards the feed at 25 °C and 35 °C, in which cases the adsorption started to slow down significantly only during the few final hours of the experiment (see Supporting Information Fig. S2).

At 12 °C, the adsorption rate was clearly lower than at higher temperatures. As shown in Fig. 5a, at 12 °C, the CO_2 concentration increases quickly in the first minutes of the run, but then the increase slows down. It could be observed in this experiment that the CO_2 concentration and, thus, the CO_2 uptake increased for the whole duration of the 12-hour adsorption phase (Fig. S2). Additionally, the adsorption rate at 12 °C stays at a higher level during 5–10 h from the start of adsorption, decreasing from around 0.032 to 0.017 $mmol_{CO2}/(g_{sorbent} \cdot h)$ (see Supporting Information S.10). In comparison, at 25 °C, the adsorption rate drops from 0.035 to around 0.008 $mmol_{CO2}/(g_{sorbent} \cdot h)$ over the same period. Thus, it seems that the sample did not reach saturation at the end of the 12 °C adsorption experiment compared to the 25 °C and higher adsorption temperatures. Still, as shown in Fig. 6, the final CO_2 uptake is lower at 12 °C compared to 25, 35, and even 52 °C due to a much lower adsorption rate in the initial hours of adsorption (see Fig. 5a). Notably, adsorption/desorption capacities measured at 25 °C and 35 °C were approximately the same, around 0.9 $mmol_{CO2}/g_{sorbent}$ in the long cyclic run. The results were similar in the adsorption experiments 5–7 (see Table 1), where the adsorption/desorption capacities were approximately 0.9–1.0 $mmol_{CO2}/g_{sorbent}$ and 1.0–1.1 $mmol_{CO2}/g_{sorbent}$ at 25 and 35 °C, respectively.

Table 1

Adsorption-desorption capacities of the ED@MOF-74 in different experiments and conditions. Experiments 2–7 were done in successive cycles using the same sample.

Experiment	c_{H2O} (vol%)	t_{ads} (h)	T_{ads} (°C)	T_{des} (°C)	$q_{CO2,ads}$ ($mmol_{CO2}/g$)			$q_{CO2,des}$ ($mmol_{CO2}/g$)			$q_{H2O,ads}$ ($mmol_{H2O}/g$)			$q_{H2O,des}$ ($mmol_{H2O}/g$)		
1	0	12	25	100	0.42	±	0.05	0.36	±	0.03						
2	0	16	26	120	0.67	±	0.08	0.77	±	0.06						
3	1.6	16	25	120	1.79	±	0.22	1.68	±	0.14	11.60	±	0.81	11.76	±	0.42
4	1.6	16	35	120	0.66	±	0.08	0.77	±	0.06	8.42	±	0.59	9.44	±	0.33
5	0	16	35	120	1.14	±	0.14	0.98	±	0.08						
6	0	16	25	120	0.98	±	0.12	0.87	±	0.07						
7	0	16	25	120	0.90	±	0.11	0.84	±	0.07						
Dry cyclic[a]	0	5	25	120	0.82	±	0.10	0.75	±	0.06						
Humid cyclic[b]	1.9	5	25	120	1.07	±	0.13	0.90	±	0.07	10.08	±	0.7	10.95	±	0.39
Long cyclic	0	12	25	120	0.91	±	0.11	0.94	±	0.08						
Long cyclic	0	12	35	120	0.95	±	0.12	0.89	±	0.07						

[a] The highest result of the dry cyclic experiment.
[b] Result from cycle 1 of humid cycling. The same sample was used as in the dry cyclic run.
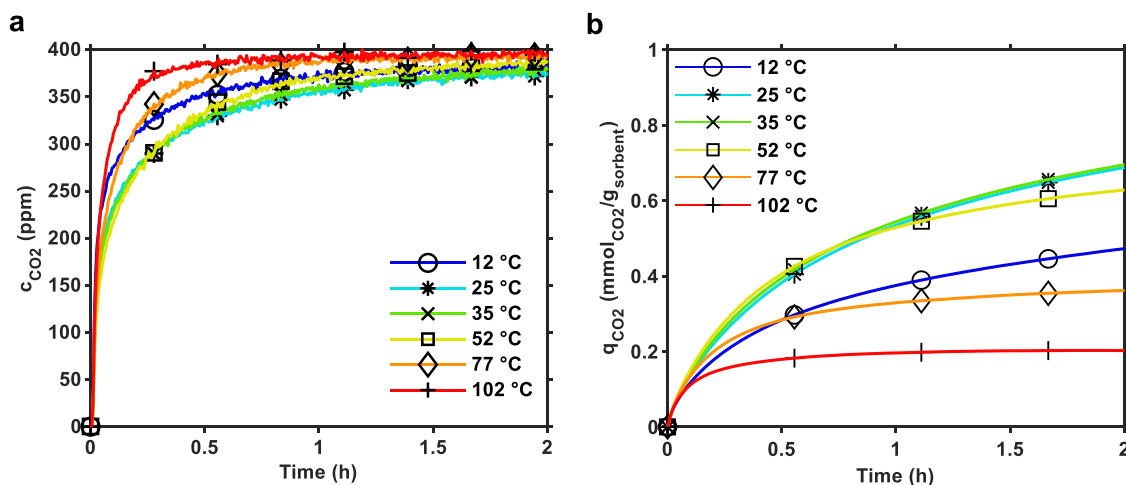
Fig. 5. Experimental a) CO$_2$ concentration and b) uptake profiles at different adsorption temperatures from the first two hours of adsorption. Feed was approximately 400 ppmv CO$_2$ in N$_2$. The uptake data in b) is not corrected with empty column breakthrough data.
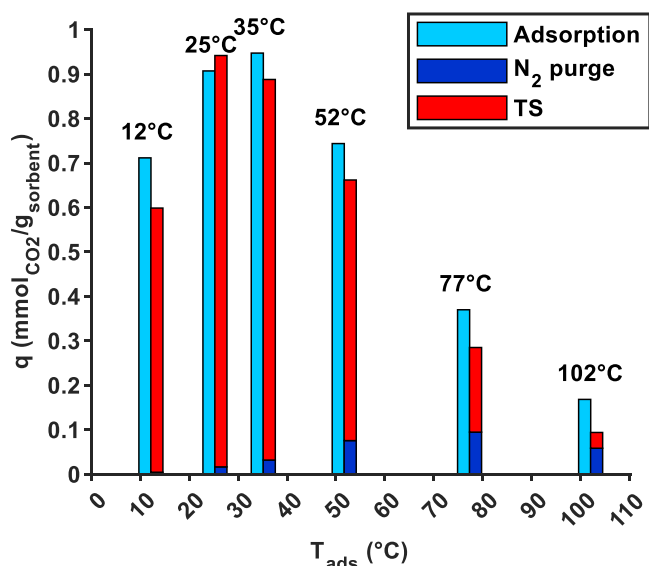

Fig. 6. Experimental CO$_2$ adsorption and desorption capacities at different adsorption temperatures from approximately 400 ppm dry CO$_2$. Adsorption time was 12 h. Temperature swing (TS) was done at 120 °C.

These results suggest that the ED@MOF-74 suffers from a limited adsorption rate in the adsorption of CO$_2$ from the air, especially at temperatures lower than 25 °C. These results could have implications for the practical applicability of the sorbent for DAC in cold climates. Although the measured adsorption capacities at the lowest adsorption temperatures could be higher with longer adsorption times, a prolonged adsorption phase can drastically reduce the CO$_2$ productivity of the DAC process [48] and thus increase the cost of captured CO$_2$.

The measured adsorption capacities at different temperatures shown in Fig. 6 can be utilized to estimate the achievable working capacity in a temperature-swing adsorption (TSA) process. As an example, from the measured adsorption capacities, with adsorption at 25 °C and desorption at 77 °C or 102 °C resulted in working capacities of around 0.54 mmol$_{CO2}$/g$_{sorbent}$ or 0.74 mmol$_{CO2}$/g$_{sorbent}$, respectively. These correspond to approximately 59% or 81% of the adsorption capacity at 25 °C, respectively. In this regard, the ED@MOF-74 differs significantly from the pore-expanded version of Mg-MOF-74 modified with ED [en-Mg$_2$(dobpdc)], for which CO$_2$ adsorption tests at 0.39 mbar resulted in 2.83 mmol$_{CO2}$/g$_{sorbent}$, 0.11 mmol$_{CO2}$/g$_{sorbent}$, and negligible adsorption

at 25 °C, 50 °C and 75 °C, respectively [49]. In an actual DAC process, the desorption is typically achieved through either temperature-vacuum swing (TVS) [50,51], steam-stripping [52], or a combination of these [53–55]. The comparison of the working capacities based on adsorption capacities measured in dry TSA/TCSA conditions has limited practical utility but can provide a preliminary estimate of the working temperature range. For example, it is clear that if less than 60% of the adsorption capacity is achievable with a regeneration temperature of 77 °C in TSA, it is likely that a higher temperature is required in a TVSA process to achieve a similar working capacity, where the achievable working capacity can be much lower than in TSA operation [42]. On the other hand, steam acts as both the stripping gas and the conveyor of heat, which can result in a higher working capacity if steam-stripping regeneration is used. Therefore, using a regeneration temperature of 100 °C in a steam-stripping operation may result in a higher working/adsorption capacity ratio than 81%.

The impact of adsorption temperature was also investigated in an adsorption isobar experiment, where the feed was in constant condition while only the temperature was varied. The results of this run were similar to those presented above, although the measured CO$_2$ uptakes were slightly lower in the adsorption isobar experiment. However, at 25 °C, the CO$_2$ uptake was lower than at around 50 °C, which contradicts the results shown in Fig. 6. The results are different due to the much shorter adsorption times, which likely explains why adsorption was not close to equilibrium. In the adsorption isobar experiment, adsorption was also measured at 120 °C, where the CO$_2$ uptake was already lower than 0.1 mmol$_{CO2}$/g$_{sorbent}$. It was also found that after N$_2$ purge at 120 °C, increasing the desorption temperature beyond 133 °C did not result in any significant further desorption. Based on these results, in terms of working capacity, it does not seem reasonable to use a temperature higher than 120 °C to regenerate the ED@MOF-74. However, as previously discussed, the productivity of DAC is greatly affected by the length of adsorption-desorption cycles, so higher regeneration temperature may be beneficial from a kinetic and productivity point-of-view. Moreover, other processes, such as TVSA, may benefit more from a higher desorption temperature. The adsorption isobar results are shown and discussed in more detail in the Supporting Information.

3.2.2. Effect of humidity

In DAC processes, CO$_2$/water co-adsorption is an unavoidable challenge because ambient air always contains a certain humidity, up to 84 g/m^3 worldwide [30]. Humidity can change the type of reaction in amine-based sorbents, shifting the reaction product of CO$_2$ and amines from ammonium carbamate to species such as bicarbonate or hydronium carbamate, thus increasing the CO$_2$ adsorption capacity [41,56,57].

On the other hand, co-adsorbed water causes parasitic heat loss during desorption, significantly increasing the energy demand of the DAC process [48]. Additionally, most MOFs tend to experience a reduction in crystallinity and BET surface area when exposed to humid conditions [58]. However, it is known that the stabilization of MOFs with exposed metal cations under humid conditions is often improved by functionalization with amines. Generally, for amine-containing adsorbents, the formation of urea leads to the deactivation of amines under dry conditions, thus reducing CO_2 capacity. However, under humid conditions, urea formation is obstructed [59], which may, in turn, improve the water stability of the amine-functionalized adsorbents [60].

It is well established that studying humid CO_2 adsorption is vital when assessing materials for the DAC potential. However, literature is still scarce in this aspect, particularly in the case of amine-modified MOFs, and the nearest examples can usually be found in articles related to post-combustion capture. For example, a study by Mason et *al.* [61] investigated a series of MOF systems for CO_2 adsorption using a multicomponent adsorption analyzer considering a gas mixture composed of water, CO_2, and N_2. Amine appended CuBTTri demonstrated a slightly decreased equilibrium CO_2 capacity after exposure to water. On the other hand, CO_2 adsorption on mmen-Mg$_2$(dobpdc) was promoted in the presence of 14% CO_2/N_2 up to 32% RH conditions and found to be 14% higher (nearly 4.2 mmol$_{CO2}$/g$_{sorbent}$) compared to dry

conditions. Remarkably, the isostructural nickel analogue, mmen-Ni$_2$(-dobpdc), which has been reported not to undergo carbamate insertion in CO_2 presence, was found to display a noticeable enhancement in the CO_2 capture, close to 3-fold, in comparison to the dry case [61]. In another example, after exposure to humid conditions (100% RH), MOFs possessing diamines with side alkyl substituents, such as men-Mg$_2$(dobpdc) and den-Mg$_2$(dobpdc), yielded only a marginal difference in CO_2 capacity. In comparison, CO_2 capacity of en-Mg$_2$(dobpdc) decreased roughly by 67% (4.30 *versus* 2.88 mmol$_{CO2}$/g$_{sorbent}$, under 15% CO_2/N_2 at 40 °C). The hydrolytic stability was ascribed to the fact that branched diamines contain methyl groups, which can help safeguard the Mg–N bonds from hydrolyzing [56,62].

For ED@MOF-74, as indicated in Table 1 above, the highest adsorption capacity of approximately 1.8 mmol$_{CO2}$/g$_{sorbent}$ was obtained in humid conditions at 25 °C, using a feed with 400 ppm CO_2 with around 2 vol% humidity, demonstrating the positive impact of humidity. However, at 35 °C, the adsorption capacity decreased to around 0.7 mmol$_{CO2}$/g$_{sorbent}$, marking a considerable capacity decrease of about 60% in only a 10 °C temperature swing. Nonetheless, as discussed in the previous section, no reduction in CO_2 capacity was found in dry adsorption conditions at 25 °C compared to 35 °C. Kwon et *al.* [63] also made a similar observation for aminopolymer-impregnated meso/macroporous silica sorbent under DAC conditions, suggesting

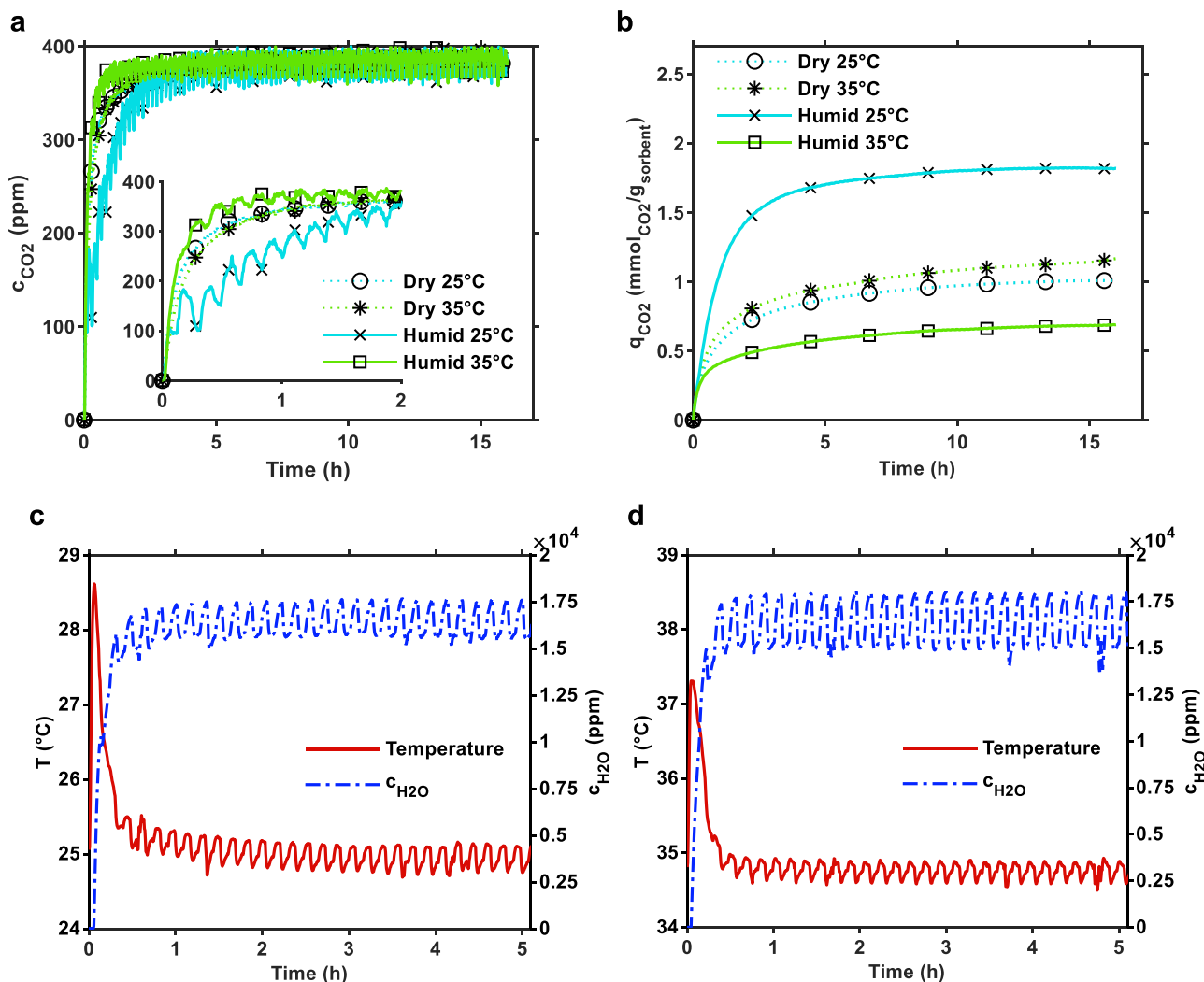**Fig. 7.** Experimental a) CO_2 concentration; b) CO_2 uptake profiles in dry and humid conditions at 25 °C and 35 °C. Temperature and H_2O concentration from the first 5 h of adsorption in the humid experiments c) at 25 °C; d) 35 °C. Feed was approximately 400 ppmv CO_2 in N_2. The uptake data in b) is not corrected with empty column breakthrough data. The markers are a guide to the eye.

water vapor presence mitigates kinetic limitations.

Fig. 7 compares adsorption breakthrough data in dry and humid conditions. As shown in Fig. 7a, the CO_2 concentration increases significantly slower towards the feed in the humid 25 °C experiment compared to dry conditions or the humid 35 °C. Consequently, the uptake curve in Fig. 7b shows a much higher adsorption rate during the first two hours in the humid 25 °C experiment. This is also shown in the moving average adsorption rate plots in Supplementary Information (S.10). At 25 °C in humid conditions, the adsorption rate starts from 1.34 mmol$_{CO2}$/(g$_{sorbent}$·h) and drops to around 1.06 mmol$_{CO2}$/(g$_{sorbent}$·h) after 30 min of adsorption (around 21% drop). On the other hand, in dry conditions at 25 °C, the respective values are 0.82 and 0.55 mmol$_{CO2}$/(g$_{sorbent}$·h) (33% drop). The adsorption rate in humid conditions clearly exceeds the adsorption rate measured for an amine-functionalized resin in similar CO_2 and H_2O concentration conditions and adsorption temperature, which was 0.88 mmol$_{CO2}$/(g$_{sorbent}$·h) [41] (calculated from the first 30 min). However, it should be noted that the gas/solid ratio in this work was around twice compared to [41,42] and the amino resin had a much larger particle size median of 600 μm [64] compared to an average of 0.4 μm for the ED@MOF-74 (measured from SEM). In pelletized form, it is expected that the ED@MOF-74 has a slower adsorption rate than that measured here.

Fig. 7c and d show the temperature peaks observed in the humid experiments. No clearly observable temperature peak was seen in the dry experiments. Additionally, as shown in Table 1, the measured H_2O adsorption and desorption capacities were several times higher than the CO_2 capacities. Therefore, it can be construed that the measured temperature increase during adsorption was due to the adsorption of H_2O rather than increased CO_2 uptake. Similar findings were found for the amino resin examined in earlier work [41]. However, as mentioned in Section 2.3, the temperature probe was above the sample; thus, the temperature profiles shown in Fig. 7 do not represent the actual sample temperature. Therefore, the temperature increase caused by CO_2 may not be evident due to the dispersion of the temperature profile. The H_2O concentration profiles are also displayed in Fig. 7c and d. Notably, the "noisy" behavior of the CO_2 profile in Fig. 7a is due to the highly variable H_2O concentration. This is due to air in the capillaries of the humidity calibrator used to humidify the feed, which has also been discussed in earlier work [41].

Fig. 8 shows the adsorption breakthrough data in dry and humid conditions in a multi-cycle experiment. Since the cycling was done with the same sample by continuing with humid cycling after dry cycling, the data of the last dry cycle and the first humid cycle are compared here. Notably, while the CO_2 adsorption uptakes calculated from the first 5 h of adsorption between different experiments in dry conditions matched, in humid conditions, there is a significant difference in CO_2 adsorption uptakes between the two experiments shown in Figs. 7 and 8, approximately 1.8 *vs.* 1.1 mmol$_{CO2}$/g$_{sorbent}$, respectively. The main reason for
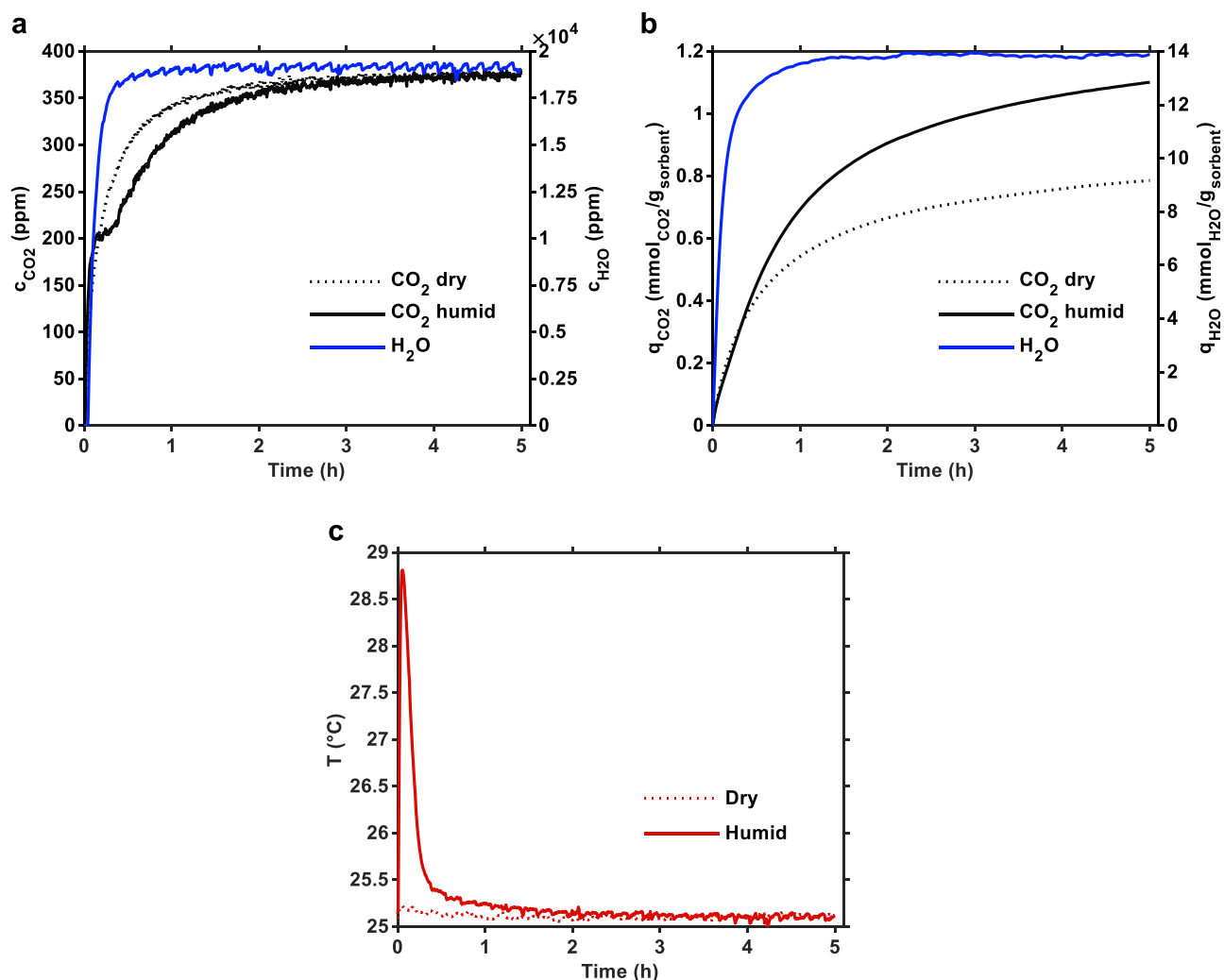
Fig. 8. Experimental a) CO_2 and H_2O concentration; b) CO_2 and H_2O uptake; c) temperature profiles from the adsorption phase of two consecutive adsorption-desorption cycles in dry and humid conditions using the same sample. The dry data is from the last cycle of the dry cyclic stability experiment, while the humid data is from the first cycle of the humid cyclic stability experiment. The uptake data in b) is not corrected with empty column breakthrough data.

the much lower adsorption uptake measured in the multi-cycle experiment is that the sample had undergone 18 dry adsorption-desorption cycles before initiating the humid cycling. The drop in capacity and stability of the ED@MOF-74 is discussed in more detail in the next section below (3.3.2).

The results shown in Fig. 8 allow a better comparison of the breakthrough curve shape between dry and humid conditions than in Fig. 7 due to a much steadier H_2O concentration profile during the humid run. It is shown in Fig. 8a that unlike in the dry run, in humid conditions, the CO_2 concentration first increases quickly to around 200 ppm but then continues on a much slower path toward the feed. This can be explained by the temperature increase shown in Fig. 8c, which slows down the adsorption of CO_2 during the first 20–30 min of adsorption. The temperature increase in this experiment is reasonably similar to that shown in Fig. 7, which is almost 4 °C. Additionally, the measured H_2O adsorption/desorption capacities were around 12 mmol$_{H2O}$/g$_{sorbent}$ in experiment 3 (see Table 1) and 10–11 mmol$_{H2O}$/g$_{sorbent}$ in the multi-cycle experiment. This is around double to that measured for the proprietary amino resin studied earlier [41] or the commercial Lewatit VP OC 1065 [65]. As for MOFs, Mason et al. [61] compared the performance of different MOFs under conditions that are pertinent to power plant flue gas and reported H_2O uptake up to 9.5, 5.4, 14.2, 18.2 mmol$_{H2O}$/g$_{sorbent}$ for mmen-Mg$_2$(dobpdc), mmen-CuBTTri, Mg$_2$(dobdc) and HKUST-1, respectively. Thus, consistent with ED@MOF-74, H_2O adsorption capacities in these hybrid materials remained more dominant than the corresponding CO_2 capacities.

The adsorption of H_2O can thus have three significant practical implications for using this adsorbent for DAC. Firstly, a high amount of adsorbed H_2O significantly enhances the regeneration energy requirement of the DAC process. For example, suppose the q_{H2O}/q_{CO2} ratio is 6.4, as in experiment 3 (see Table 1). In that case, the isosteric heat of H_2O adsorption using the heat of H_2O vaporization of 44 kJ/mol at 25 °C constitutes around 6.4 MJ/kg$_{CO2}$. The latent heat due to H_2O desorption is thus a significant part of the total energy requirement of DAC, with upper limits estimated from around 12 MJ/kg$_{CO2}$ [53] to 19 MJ/kg$_{CO2}$ [66]. The second practical implication also arises from the isosteric heat of H_2O adsorption since, as shown in the data above, the H_2O adsorption causes a temperature increase, which reduces the adsorption of CO_2. In the results shown here, the heat transfer in the adsorption column can be regarded as reasonably optimal due to the small diameter column, which may not be true for process-scale DAC adsorption columns. Therefore, this phenomenon is likely more prominent in the process-scale DAC and may lead to a reduced adsorption rate in the beginning, causing a delay in the adsorption phase or reduced working capacity and thus reduced productivity of CO_2. Analogously, while the adsorption heat may delay the adsorption phase, the cooling effect during the desorption of the gases may delay the regeneration phase. It should also be considered that the laboratory-scale adsorption column was actively cooled during adsorption through the column wall using a heat-transfer fluid. Therefore, with adsorbents that capture significant amounts of H_2O, the heat transfer and the active cooling of the adsorption column during adsorption become more important. The third and possibly the most critical implication of humidity for the long-term use of DAC is the possible degradation of the MOF, which is investigated in the next section.

3.3. Cyclic stability

The assessment of CO_2 adsorption during repetitive adsorption-desorption cycles is the true measure in evaluating the material's tolerance to operating conditions, its long-term viability for a practical capture process, and minimizing the cost related to DAC operation. To assess the stability of the ED@MOF-74, dry and humid cyclic adsorption-desorption experiments were conducted, after which the samples were analyzed with PXRD, FT-IR, and EA. In total, there were two characterized samples. The first sample underwent 18 dry and 18 humid

adsorption/desorption cycles, and the second sample underwent the dry adsorption isobar and long cyclic tests. In Section 3.3.2, these two samples are referred to as "ED@MOF-74-CO$_2$-humid" and "ED@MOF-74-CO$_2$-dry" respectively.

3.3.1. Cyclic DAC experiments

Intriguingly, as shown in Fig. 9, it was found that the cyclic adsorption and desorption capacities were lower in the first adsorption-desorption cycles compared to the following ones. This finding was consistent with the preliminary experiments, where the adsorption and desorption capacities of experiment 2 were lower than in experiments 6 and 7, which were conducted in similar conditions and used the same sample. After the fourth cycle, the cyclic capacities seem to stabilize. In cycles 5 to 18, a slightly decreasing trend can be observed in the cyclic capacities. The adsorption and desorption capacities drop from around 0.85 and 0.75 mmol$_{CO2}$/g$_{sorbent}$ in the 5th cycle to around 0.79 and 0.73 mmol$_{CO2}$/g$_{sorbent}$ in the 18th cycle, respectively. Calculated from the desorption capacity values, the drop in capacity corresponds to around 2.7%, or 0.2%/cycle. This capacity drop rate is comparable to the 0.18%/cycle measured for a proprietary amino resin over 19 dry TCSA cycles with the same device [42].

Even though the regeneration was deemed complete between cycles, it is possible that the lower cyclic capacities observed in the first four cycles are due to incomplete regeneration and thus reaching a cyclic steady state by cycle nr. 5. Another reason may be that the sample required a more extended activation due to blockage of some of the pores with physically bound ethylenediamine, which was then removed after a few cycles with regeneration temperature near the evaporation temperature of free ED (see TGA results in Section 3.1). This could also explain why higher results were gained in the preliminary experiments after a few adsorption-desorption cycles, as discussed in Section 3.2. To avoid this from affecting the results of the humid cycling, the humid cycling was continued with the same sample after the last dry cycle.

Although the capacity drop observed in the dry cycling was rather moderate, the humid adsorption and desorption capacities at the start of the humid cycling were much lower compared to the preliminary experiment done in similar conditions, as discussed in Section 3.2.2. Thus, it appears that degradation of the adsorption sites was more prominent during the dry cycling than what could be observed based on the evolution of the measured CO_2 capacities. One reason for this could
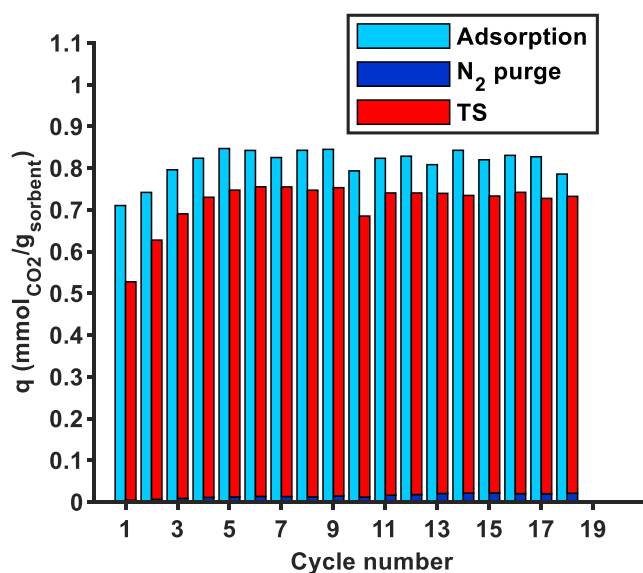

Fig. 9. Experimental CO_2 adsorption and desorption capacities in the repeated cycles of dry temperature-concentration swing adsorption. Adsorption was conducted at 25 °C with around 400 ppmv CO_2. Desorption was conducted at 120 °C using pure N_2 feed.

be that humidity enables the adsorption of CO_2 on amine sites that are both more susceptible to degradation and cannot adsorb CO_2 in dry conditions. When such amines are degraded due to, *e.g.,* the high regeneration temperature, the drop in adsorption capacity is not observed in dry cycles. Humidity may disrupt the H-bonded networks between adjacent primary amine groups, thereby incrementing CO_2 binding sites (more accessible free amines) [61,67–69]. Therefore, a fair amount of the diamine molecules exist in the MOF pores as free amines, thus being unbound to the metal sites, and thereby cannot adsorb CO_2 in dry conditions. Such amines are then easily leached out due to evaporation by heating, which may justify why the CO_2 capacity at the start of the humid cycling was much lower than in experiment 3. The existence of free ED is evidenced by the TGA results in Section 3.1.

A drastic decline in CO_2 and H_2O capacities could be observed in humid conditions, as shown in Fig. 10. The cyclic CO_2 capacity, as shown in Fig. 10a, drops rapidly at the beginning but slows down after the 7th cycle. The CO_2 desorption capacity drops from around 0.90 to 0.44 $mmol_{CO2}/g_{sorbent}$ in the first 7 cycles, corresponding to over 50% drop, around 7%/cycle. However, from the 7th to the 18th cycle, the CO_2 desorption capacity drops to around 0.23 $mmol_{CO2}/g_{sorbent}$, corresponding to a drop rate of 4%/cycle. In total, the desorption capacity decreased by around 74% as compared to the first cycle. On the other hand, the decreasing trend in the cyclic H_2O capacities in Fig. 10b seems somewhat constant throughout the experiment, although it slows down in the last few cycles. The desorption H_2O capacity drops from around 11 to 8.5 $mmol_{H2O}/g_{sorbent}$, corresponding to around a 23% drop, or 1.3%/cycle. The major loss of CO_2 capacity may refer to significant changes in the underlying framework or the loss of active amine sites. The cause of the capacity loss was studied by characterizing the samples after the cycling tests, as shown in the next Section (3.3.2).

3.3.2. Characterization of ED@MOF-74 post-cycling

The progressive decrease in capacity after repeated tests under both dry and humid conditions can be most likely explained by the partial structural collapse, or the material propensity towards amine loss upon regeneration, or the adverse impact of moisture. PXRD, FT-IR, and EA were conducted after subsequent cyclic tests to corroborate the structural changes and verify the nitrogen content in the post-cycling samples to support this interpretation. Upon adsorption\desorption cycling under dry and humid conditions, both ED@MOF-74 samples experienced a dramatic reduction in crystallinity, as evidenced by the broadened and markedly lowered intensities of characteristic diffraction peaks, as can be seen in the PXRD pattern shown in Fig. 11. The decrease in crystallinity may be plausibly caused by the continuous adsorption and desorption cycling, resulting in the fractionation of bigger crystals

into smaller ones and causing crystal defects. Nevertheless, in our study, the PXRD pattern still displays the retention of original MOF diffraction peaks (Fig. S5). Such retention of the PXRD pattern is possible even with a major change in the MOF structure. For example, Kumar et *al.* [58] found that the presence of moisture caused an appreciable decline in the adsorption performance of Mg-MOF-74. While its PXRD pattern exhibited no change, the BET surface area decreased to 74% after one day of humidity exposure and became negligible (6 m^2/g) after prolonged exposure (7 or 14 days), implying partial pore blockage, possibly by rearrangement of amine groups or pore collapse. Literature suggests that the considerable loss of surface area provides strong evidence for amorphization and partial structural degradation [70].

Accordingly, as seen in Fig. 12, FT-IR spectra of all the samples, regardless of whether from dry or humid conditions, exhibit a significant loss of the spectral bands' intensity associated with the amine modes, particularly the doublet attributed to ν_s and ν_{as} (N-H) stretching modes of amines (as discussed earlier). This indeed suggests that there was some amine loss during CO_2 capture/releasing cycles, which was confirmed by elemental analysis (see Table S7). In Fig. 12, it can be observed that the bands in ED@MOF-74 samples associated with the amine modes are shifted to 3281 cm^{-1} for ED@MOF-74-CO_2-humid, and 3309 cm^{-1} for ED@MOF-74-CO_2-dry, respectively. Additionally, a new weak shoulder has been registered roughly around 1680 cm^{-1} on both the post adsorption\desorption cycling samples. This band has been previously attributed to the $O=C=O$ bending mode during chemisorption [71,72]. Therefore, it is feasible that a reduction in CO_2 capacity could result from a small portion of the adsorbed CO_2 remaining in a stable and strongly chemisorbed form in the ED@MOF-74, making the adsorption–desorption process partially non-reversible. However, there is insufficient conclusive evidence for this interpretation as the shoulder observed is very weak, possibly due to H-bonding, and other bands are not well distinguishable. Moreover, it is very challenging to detect infrared bands of the adsorbed species that produce signals typically between $1800 - 1200 \ cm^{-1}$[66] due to the overlapping of bands by the organic bridging linker in this region.

It needs to be mentioned that the downward trend in capacity because of the diamine leaching has also been observed in other diamine-appended MOF systems [34,73–76]. For example, Adil et *al.* [34] exploited the performance stability of amine-functionalized material under humid conditions by using the flow-mode breakthrough system, simulating practical post-combustion carbon capture scenarios. The authors demonstrated that mmen-Mg_2(dobpdc) is not stable in cyclic mode, reflected by a notable decrease (~30%) in CO_2 retention time observed after five cycles, suggesting the amine's detachment from OMSs as water molecules compete for them. They explained that the
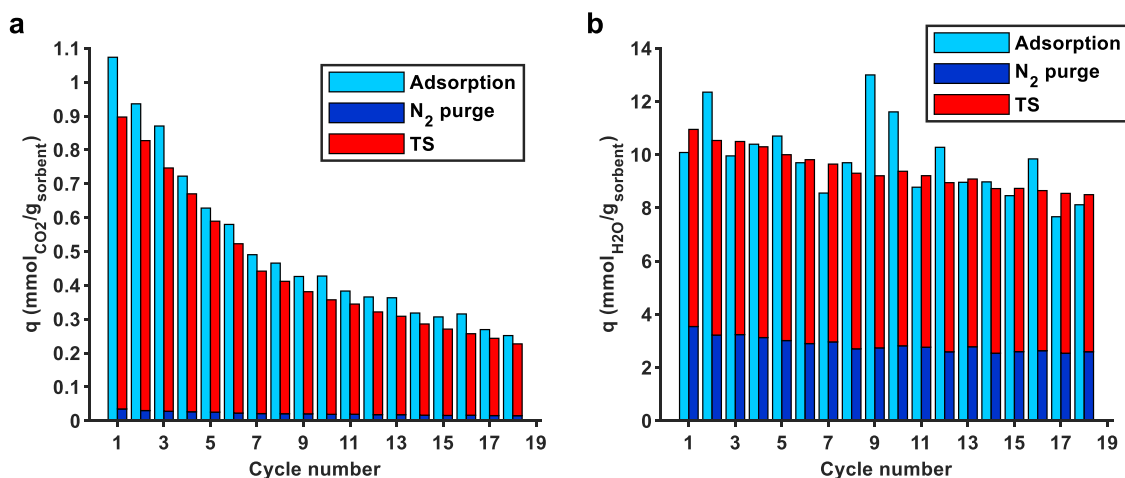

Fig. 10. Adsorption and desorption capacities in the repeated cycles of humid temperature-concentration swing adsorption of a) CO_2 and b) H_2O. Adsorption was conducted at 25 °C with around 400 ppmv CO_2 and 2 vol% H_2O in N_2. Desorption was conducted at 120 °C using pure N_2 feed.
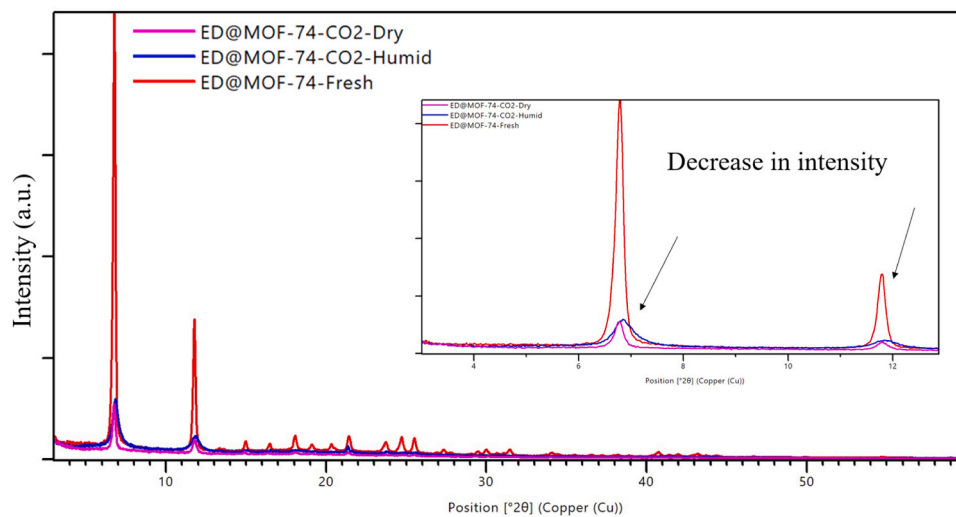
Fig. 11. PXRD pattern of ED@MOF-74 before and after adsorption/desorption cycling under dry and humid conditions.
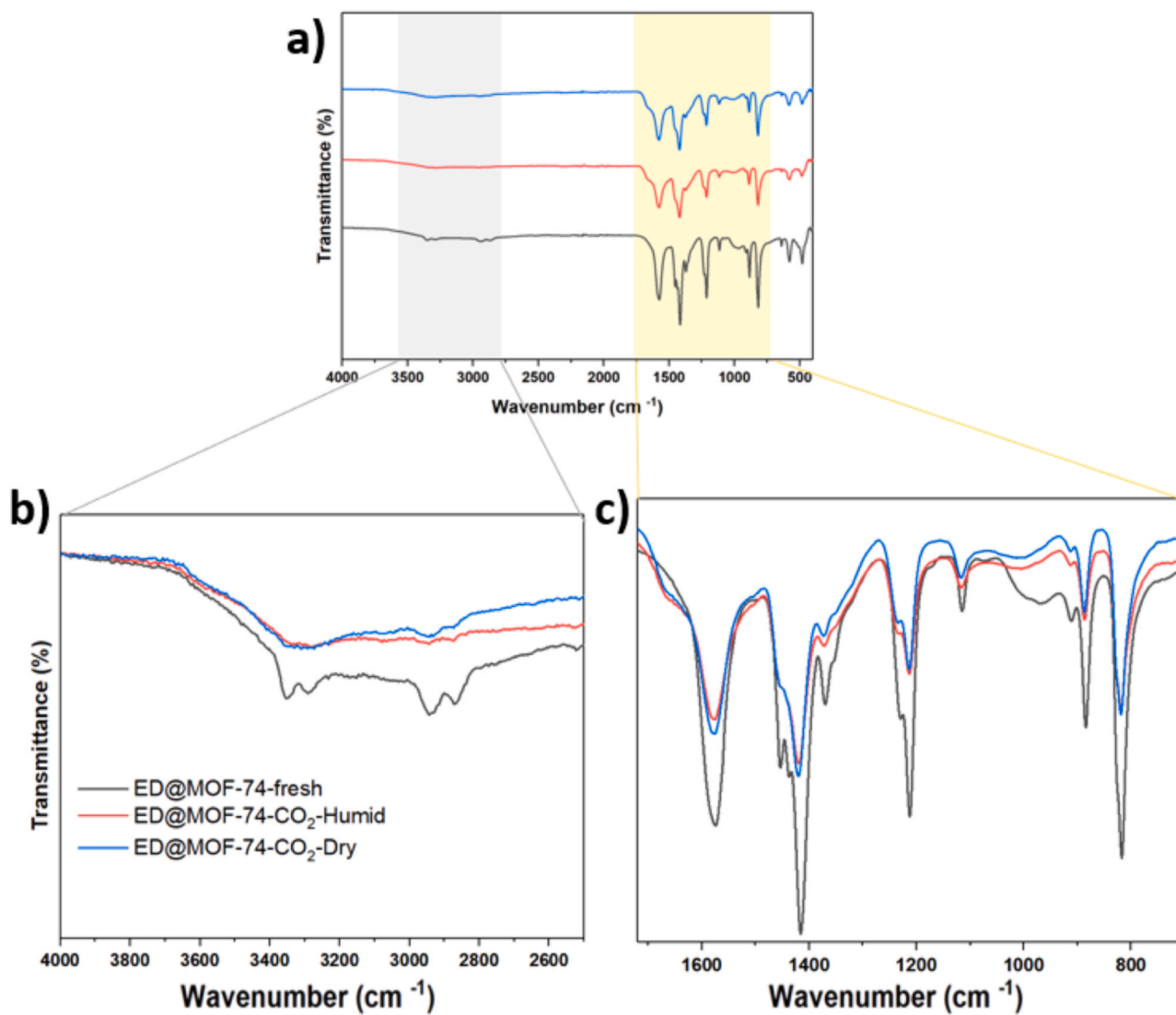

Fig. 12. FT-IR of ED@MOF-74 before and after adsorption/desorption cycling under dry and humid conditions a) complete spectra, magnification of the b) 3500 to 2600 cm^{-1} and c) 1700 to 800 cm^{-1} regions.

relatively strong binding energy between H_2O and Mg^{2+} compared to Mg–amine disrupts coordinated diamines, thus leading to the amine loss and gradual reduction in CO_2 uptake [34]. In the literature, the degradation of amine-supported adsorbents was investigated under dry conditions and CO_2 capacity loss was correlated with the deactivation of primary amines by urea species formation [59,77].

Since amine-functionalization holds tremendous promise for atmospheric CO_2 capture, future studies should pay close attention to humid instability issues to further enhance the performance of these desirable adsorbent systems under humid DAC conditions. Coating diamine-functionalized MOFs with polymers that induce hydrophobic properties is recommended to reduce the dramatic impact of water vapor [78, 79]. The adsorbent Choe et al. [74] studied relied on the fabrication of diamine-appended Mg2(dobpdc)-alumina\silane\epoxide composites. They concluded that the epoxide's ring-opening reaction with diamines appended to exposed metal cations afforded improved hydrophobicity, hindered water vapor penetration into the pores, and reduced the diamine volatilization.

4. Conclusions

In the present work, we investigated the effectiveness of ED@MOF-74 for direct air capture using an automated fixed-bed adsorption setup combined with physicochemical characterization. We evaluated the carbon capture performance of the adsorbent in both dry and humid DAC-relevant conditions and tested its stability through adsorption/desorption TCSA cycling. Our evaluation included a more comprehensive range of operating conditions compared to existing literature, such as temperature and humidity, which were found to impact the ED@MOF-74 performance dramatically.

In dry conditions using 12-hour adsorption, the measured CO_2 uptake dropped progressively at adsorption temperatures higher than 35 °C. The adsorption/desorption capacities registered at 25 °C and 35 °C were similar, around 0.9 $mmol_{CO2}/g_{sorbent}$. However, at 12 °C, the CO_2 uptake was lowered to roughly 0.7 $mmol_{CO2}/g_{sorbent}$. It was noted that the sample was not reaching saturation at the end of the 12 °C adsorption experiment compared to 25 °C or at higher temperatures used, suggesting that ED@MOF-74 could suffer from mass-transfer limitations in the CO_2 capture from the air at temperatures much below 25 °C. In humid conditions at 25 °C, the difference in CO_2 uptake under dry *vs.* humid conditions was the highest, measuring 1.8 $mmol_{CO2}/g_{sorbent}$ using a feed with 400 ppm CO_2 and around 2 vol% humidity. However, in contrast to the trend observed in the dry CO_2 stream at a temperature of 35 °C, the adsorption capacity decreased drastically to around 0.7 $mmol_{CO2}/g_{sorbent}$, marking a decline of nearly 60% in only a 10 °C temperature swing. Additionally, the amount of adsorbed H_2O was multiple times that of CO_2, being around 10–11 $mmol_{H2O}/g_{sorbent}$. In consecutive TCSA cycles using the ED@MOF-74, only a small cyclic capacity drop of around 3% occurred in 18 cycles during dry conditions. However, over continued cycling at 2 vol% humidity, the capacity drop was significantly pronounced, leading to around 74% loss of CO_2 uptake compared to the first humid cycle result.

Characterization of ED@MOF-74 following dry experiments and dry \humid TCSA cycling using PXRD and EA analyses revealed that the samples lost both crystallinity and nitrogen content. Furthermore, the FT-IR studies illustrated that both samples experienced a loss of intensity in the spectral bands associated with amines compared to the fresh ED@MOF-74. As demonstrated by the TGA results, a significant portion of the ethylenediamine in the ED@MOF-74 existed in the form of free amines, volatilizing slightly above 120 °C. Altogether, characterization results suggest that the material propensity towards amine loss could be responsible for the performance decrease after successive TCSA cycles, and here, we propose two potential mechanisms for the amine loss. Firstly, in dry conditions, the free amines present in the sample are progressively removed after repeated temperature elevation from the

adsorption temperature up to 120 °C. Secondly, in humid conditions, the water molecules may strip the ED groups from the grafted sites after repeated humid cycles. It is also plausible that because there was a high amount of adsorbed H_2O, ED might have dissolved in the water and then left as droplets during desorption.

This study shows that the ED@MOF-74 has multiple challenges when it comes to its real-life application as a viable DAC adsorbent, especially due to the high required desorption temperature, low adsorption rate at low temperature, high H_2O uptake, and structural degradation. Decreasing the regeneration temperature may prevent degradation in dry conditions but will significantly compromise the achievable cyclic working capacity, especially if temperature-vacuum swing adsorption is used. Based on humid experiments at 25 °C and 35 °C, humidity facilitates the regeneration process, which could mean a lower regeneration temperature could be used in humid conditions. However, humidity also clearly renders the adsorbent useless over multiple cycles through active amine site loss, which may promote using this adsorbent in significantly dried air. Another reason against applying the adsorbent in a high-humidity climate is the tendency to capture high amounts of H_2O, increasing the energy requirement of the process. On the other hand, application in dry air usually means cold, sub-zero conditions, which seem to entail kinetic limitations. Moreover, the process-scale application of the MOF would require either pelletizing or coating the adsorbent on a structured monolith. On a positive note, this study showed that even straightforward techniques can be used to achieve porous layers of CO_2-adsorbing MOFs on different substrates.

Only a few studies cover the critical aspects necessary for effectively employing MOFs in DAC-relevant conditions, specifically kinetics and stability in humid environments. Overall, the results presented in this work emphasize the necessity of directing more attention toward these aspects to incorporate amine-decorated porous supports in a realistic DAC process successfully. In future studies, more comprehensive CO_2 adsorption testing at varying relative humidities and temperatures, along with TVSA cycling, would complement the current knowledge of amine-modified MOFs. Another critical element to be systematically explored is the long-term stability of the amines. An in-depth exploration of underlying chemical and structural parameters that affect degradation would provide valuable guidance in constructing effective amine-rich sorbents. This would ensure that adsorbents maintain their high adsorption capacities over a few months, thereby maximizing the applicability of such CO_2 adsorbents for direct air capture.

CRediT authorship contribution statement

Jere Elfving: Formal analysis, Visualization, Writing – original draft, Writing – review & editing, Methodology. **Shreya Mahajan:** Investigation, Methodology, Visualization, Writing – original draft, Writing – review & editing, Formal analysis. **Manu Lahtinen:** Conceptualization, Funding acquisition, Project administration, Supervision, Writing – review & editing.

Declaration of Competing Interest

The authors declare that they have no known competing financial interests or personal relationships that could have appeared to influence the work reported in this paper.

Data availability

Data will be made available on request.

Acknowledgments

Ekholm for conducting the coating experiments and Dr. Pekka Simell for his valuable feedback and supervision during the coating experiments.

Supporting information

The Supporting Information includes details about: Structural characterization; Experimental uncertainty; The effect of feed concentration on adsorption capacity; Adsorption-desorption results; CO_2 concentration and uptake profiles at different temperatures; Adsorption isobar experiment; Characterization of ED@MOF-74 post-cycling; Coating experiments; CO_2 concentration profiles on logarithmic time scale; CO_2 adsorption rate profiles.

Notes

The authors declare no competing financial interest.

Appendix A. Supporting information

Supplementary data associated with this article can be found in the online version at doi:10.1016/j.jece.2024.112193.

References

[1] S. Fuss, W.F. Lamb, M.W. Callaghan, J. Hilaire, F. Creutzig, T. Amann, T. Beringer, W. de Oliveira Garcia, J. Hartmann, T. Khanna, G. Luderer, G.F. Nemet, J. Rogelj, P. Smith, J.L.V. Vicente, J. Wilcox, M. del Mar Zamora Dominguez, J.C. Minx, Negative emissions—Part 2: costs, potentials and side effects, Environ. Res. Lett. 13 (2018) 063002, https://doi.org/10.1088/1748-9326/aabf9f.

[2] P. Smith, S.J. Davis, F. Creutzig, S. Fuss, J. Minx, B. Gabrielle, E. Kato, R. B. Jackson, A. Cowie, E. Kriegler, D.P. van Vuuren, J. Rogelj, P. Ciais, J. Milne, J. G. Canadell, D. McCollum, G. Peters, R. Andrew, V. Krey, G. Shrestha, P. Friedlingstein, T. Gasser, A. Grübler, W.K. Heidug, M. Jonas, C.D. Jones, F. Kraxner, E. Littleton, J. Lowe, J.R. Moreira, N. Nakicenovic, M. Obersteiner, A. Patwardhan, M. Rogner, E. Rubin, A. Sharifi, A. Torvanger, Y. Yamagata, J. Edmonds, C. Yongsung, Biophysical and economic limits to negative CO_2 emissions, Nat. Clim. Chang. 6 (2016) 42–50, https://doi.org/10.1038/nclimate2870.

[3] M. Erans, E.S. Sanz-Pérez, D.P. Hanak, Z. Clulow, D.M. Reiner, G.A. Mutch, Direct air capture: process technology, techno-economic and socio-political challenges, Energy Environ. Sci. 15 (2022) 1360–1405, https://doi.org/10.1039/D1EE03523A.

[4] Y. Abdullatif, A. Sodiq, N. Mir, Y. Bicer, T. Al-Ansari, M.H. El-Naas, A.I. Amhamed, Emerging trends in direct air capture of CO_2: a review of technology options targeting net-zero emissions, RSC Adv. 13 (2023) 5687–5722, https://doi.org/10.1039/D2RA07940B.

[5] J. Fuhrman, H. McJeon, P. Patel, S.C. Doney, W.M. Shobe, A.F. Clarens, Food–energy–water implications of negative emissions technologies in a +1.5 °C future, Nat. Clim. Chang. 10 (2020) 920–927, https://doi.org/10.1038/s41558-020-0876-z.

[6] R. Gonzalez Sanchez, A. Chatzipanagi, G. Kakoulaki, M. Buffi, S. Szabo, The role of direct air capture in eu's decarbonisation and associated carbon intensity for synthetic fuels production, Energies 16 (2023) 3881, https://doi.org/10.3390/en16093881.

[7] D.W. Keith, G. Holmes, D. St. Angelo, K. Heidel, A Process for Capturing CO_2 from the atmosphere, Joule 2 (2018) 1573–1594, https://doi.org/10.1016/j.joule.2018.05.006.

[8] C.J. E. Bajamundi, J. Koponen, V. Ruuskanen, J. Elfving, A. Kosonen, J. Kauppinen, J. Ahola, Capturing CO_2 from air: technical performance and process control improvement, J. CO_2 Util. 30 (2019) 232–239, https://doi.org/10.1016/j.jcou.2019.02.002.

[9] Climeworks, subsite: "direct air capture," (2023), (n.d.). https://www.climeworks.com (accessed August 28, 2023).

[10] D. Panda, V. Kulkarni, S.K. Singh, Evaluation of amine-based solid adsorbents for direct air capture: a critical review, React. Chem. Eng. 8 (2023) 10–40, https://doi.org/10.1039/D2RE00211F.

[11] W. Lu, J.P. Sculley, D. Yuan, R. Krishna, H.-C. Zhou, Carbon dioxide capture from air using amine-grafted porous polymer networks, J. Phys. Chem. C 117 (2013) 4057–4061, https://doi.org/10.1021/jp311512q.

[12] J. Wang, H. Huang, M. Wang, L. Yao, W. Qiao, D. Long, L. Ling, Direct capture of low-concentration CO_2 on mesoporous carbon-supported solid amine adsorbents at ambient temperature, Ind. Eng. Chem. Res. 54 (2015) 5319–5327, https://doi.org/10.1021/acs.iecr.5b01060.

[13] W. Chaikittisilp, H.-J. Kim, C.W. Jones, Mesoporous alumina-supported amines as potential steam-stable adsorbents for capturing CO_2 from simulated flue gas and ambient air, Energy Fuels 25 (2011) 5528–5537, https://doi.org/10.1021/ef201224v.

[14] A. Sayari, Q. Liu, P. Mishra, Enhanced adsorption efficiency through materials design for direct air capture over supported polyethylenimine, ChemSusChem 9 (2016) 2796–2803, https://doi.org/10.1002/cssc.201600834.

[15] H. Azarabadi, K.S. Lackner, A sorbent-focused techno-economic analysis of direct air capture, Appl. Energy 250 (2019) 959–975, https://doi.org/10.1016/j.apenergy.2019.04.012.

[16] S. Mahajan, M. Lahtinen, Recent progress in metal-organic frameworks (MOFs) for CO_2 capture at different pressures, J. Environ. Chem. Eng. 10 (2022) 108930, https://doi.org/10.1016/j.jece.2022.108930.

[17] K. Sumida, D.L. Rogow, J.A. Mason, T.M. McDonald, E.D. Bloch, Z.R. Herm, T.-H. Bae, J.R. Long, Carbon dioxide capture in metal–organic frameworks, Chem. Rev. 112 (2012) 724–781, https://doi.org/10.1021/cr2003272.

[18] Ü. Kökçam-Demir, A. Goldman, L. Esrafili, M. Gharib, A. Morsali, O. Weingart, C. Janiak, Coordinatively unsaturated metal sites (open metal sites) in metal–organic frameworks: design and applications, Chem. Soc. Rev. 49 (2020) 2751–2798, https://doi.org/10.1039/C9CS00609E.

[19] E.S. Sanz-Pérez, C.R. Murdock, S.A. Didas, C.W. Jones, Direct capture of CO_2 from ambient air, Chem. Rev. 116 (2016) 11840–11876, https://doi.org/10.1021/acs.chemrev.6b00173.

[20] L. Valenzano, B. Civalleri, S. Chavan, G.T. Palomino, C.O. Areán, S. Bordiga, Computational and experimental studies on the adsorption of CO, N_2, and CO_2 on Mg-MOF-74, J. Phys. Chem. C 114 (2010) 11185–11191, https://doi.org/10.1021/jp102574f.

[21] S.R. Caskey, A.G. Wong-Foy, A.J. Matzger, Dramatic tuning of carbon dioxide uptake via metal substitution in a coordination polymer with cylindrical pores, J. Am. Chem. Soc. 130 (2008) 10870–10871, https://doi.org/10.1021/ja8036096.

[22] D. Britt, H. Furukawa, B. Wang, T.G. Glover, O.M. Yaghi, Highly efficient separation of carbon dioxide by a metal-organic framework replete with open metal sites, Proc. Natl. Acad. Sci. 106 (2009) 20637–20640, https://doi.org/10.1073/pnas.0909718106.

[23] P.D.C. Dietzel, R. Blom, H. Fjellvåg, Base-induced formation of two magnesium metal-organic framework compounds with a bifunctional tetratopic ligand, Eur. J. Inorg. Chem. (2008) 3624–3632, https://doi.org/10.1002/ejic.200701284.

[24] A.R. Millward, O.M. Yaghi, Metal−organic frameworks with exceptionally high capacity for storage of carbon dioxide at room temperature, J. Am. Chem. Soc. 127 (2005) 17998–17999, https://doi.org/10.1021/ja0570032.

[25] G.Y. Yoo, W.R. Lee, H. Jo, J. Park, J.H. Song, K.S. Lim, D. Moon, H. Jung, J. Lim, S. S. Han, Y. Jung, C.S. Hong, Adsorption of carbon dioxide on unsaturated metal sites in M_2(dobpdc) frameworks with exceptional structural stability and relation between lewis acidity and adsorption enthalpy, Chem. Eur. J. 22 (2016) 7444–7451, https://doi.org/10.1002/chem.201600189.

[26] K. Tan, S. Zuluaga, Q. Gong, Y. Gao, N. Nijem, J. Li, T. Thonhauser, Y.J. Chabal, Competitive coadsorption of CO_2 with H_2O, NH_3, SO_2, NO, NO_2, N_2, O_2, and CH_4 in M-MOF-74 (M = Mg, Co, Ni): the role of hydrogen bonding, Chem. Mater. 27 (2015) 2203–2217, https://doi.org/10.1021/acs.chemmater.5b00315.

[27] A.H. Farmahini, S. Krishnamurthy, D. Friedrich, S. Brandani, L. Sarkisov, Performance-based screening of porous materials for carbon capture, Chem. Rev. 121 (2021) 10666–10741, https://doi.org/10.1021/acs.chemrev.0c01266.

[28] J.B. DeCoste, G.W. Peterson, B.J. Schindler, K.L. Killops, M.A. Browe, J.J. Mahle, The effect of water adsorption on the structure of the carboxylate containing metal–organic frameworks Cu-BTC, Mg-MOF-74, and UiO-66, J. Mater. Chem. A 1 (2013) 11922, https://doi.org/10.1039/c3ta12497e.

[29] A.C. Kizzie, A.G. Wong-Foy, A.J. Matzger, Effect of humidity on the performance of microporous coordination polymers as adsorbents for CO_2 capture, Langmuir 27 (2011) 6368–6373, https://doi.org/10.1021/la200547k.

[30] F. Kong, G. Rim, M. Song, C. Rosu, P. Priyadarshini, R.P. Lively, M.J. Realff, C. W. Jones, Research needs targeting direct air capture of carbon dioxide: material & process performance characteristics under realistic environmental conditions, Korean J. Chem. Eng. 39 (2022) 1–19, https://doi.org/10.1007/s11814-021-0976-0.

[31] S. Choi, T. Watanabe, T.-H. Bae, D.S. Sholl, C.W. Jones, Modification of the Mg/DOBDC MOF with amines to enhance CO_2 adsorption from ultradilute gases, J. Phys. Chem. Lett. 3 (2012) 1136–1141, https://doi.org/10.1021/jz300328j.

[32] D. Andirova, Y. Lei, X. Zhao, S. Choi, Functionalization of metal-organic frameworks for enhanced stability under humid carbon dioxide capture conditions, ChemSusChem 8 (2015) 3405–3409, https://doi.org/10.1002/cssc.201500580.

[33] Y. Miao, Z. He, X. Zhu, D. Izikowitz, J. Li, Operating temperatures affect direct air capture of CO_2 in polyamine-loaded mesoporous silica, Chem. Eng. J. 426 (2021) 131875, https://doi.org/10.1016/j.cej.2021.131875.

[34] K. Adil, P.M. Bhatt, Y. Belmabkhout, S.M.T. Abtab, H. Jiang, A.H. Assen, A. Mallick, A. Cadiau, J. Aqil, M. Eddaoudi, Valuing metal-organic frameworks for postcombustion carbon capture: a benchmark study for evaluating physical adsorbents, Adv. Mater. 29 (2017) 1702953, https://doi.org/10.1002/adma.201702953.

[35] B. Yeskendir, J.-P. Dacquin, Y. Lorgouilloux, C. Courtois, S. Royer, J. Dhainaut, From metal–organic framework powders to shaped solids: recent developments and challenges, Mater. Adv. 2 (2021) 7139–7186, https://doi.org/10.1039/D1MA00630D.

[36] F. Rezaei, M.A. Sakwa-Novak, S. Bali, D.M. Duncanson, C.W. Jones, Shaping amine-based solid CO_2 adsorbents: effects of pelletization pressure on the physical and chemical properties, Microporous Mesoporous Mater. 204 (2015) 34–42, https://doi.org/10.1016/j.micromeso.2014.10.047.

[37] M.A. Sakwa-Novak, C.-J. Yoo, S. Tan, F. Rashidi, C.W. Jones, Poly(ethylenimine)-functionalized monolithic alumina honeycomb adsorbents for CO_2 capture from air, ChemSusChem 9 (2016) 1859–1868, https://doi.org/10.1002/cssc.201600404.

[38] S.M. Vornholt, S.E. Henkelis, R.E. Morris, Low temperature synthesis study of metal–organic framework CPO-27: investigating metal, solvent and base effects down to −78 °C, Dalton Trans. 46 (2017) 8298–8303, https://doi.org/10.1039/C7DT01223C.

[39] T. Degen, M. Sadki, E. Bron, U. König, G. Nénert, The highscore suite, Powder Diffr. 29 (2014) S13–S18, https://doi.org/10.1017/S0885715614000840.

[40] G.S. Pawley, Unit-cell refinement from powder diffraction scans, J. Appl. Crystallogr. 14 (1981) 357–361, https://doi.org/10.1107/S0021889881009618.

[41] J. Elfving, T. Sainio, Kinetic approach to modelling CO_2 adsorption from humid air using amine-functionalized resin: equilibrium isotherms and column dynamics, Chem. Eng. Sci. 246 (2021) 116885, https://doi.org/10.1016/j.ces.2021.116885.

[42] J. Elfving, J. Kauppinen, M. Jegoroff, V. Ruuskanen, L. Järvinen, T. Sainio, Experimental comparison of regeneration methods for CO_2 concentration from air using amine-based adsorbent, Chem. Eng. J. 404 (2021) 126337, https://doi.org/10.1016/j.cej.2020.126337.

[43] J. Elfving, 2021, Direct Capture of CO2 from Air Using Amine-functionalized Resin - Effect of Humidity in Modelling and Evaluation of Process Concepts, Lappeenranta-Lahti University of Technology LUT. https://urn.fi/URN:ISBN:978–952-335–765-5 (accessed August 10, 2023).

[44] K.I. Hadjiivanov, D.A. Panayotov, M.Y. Mihaylov, E.Z. Ivanova, K.K. Chakarova, S. M. Andonova, N.L. Drenchev, Power of infrared and Raman spectroscopies to characterize metal-organic frameworks and investigate their interaction with guest molecules, Chem. Rev. 121 (2021) 1286–1424, https://doi.org/10.1021/acs.chemrev.0c00487.

[45] T.P. Chopra, R.C. Longo, K. Cho, M.D. Halls, P. Thissen, Y.J. Chabal, Ethylenediamine grafting on oxide-free H-, 1/3 mL F-, and Cl-terminated Si(111) surfaces, Chem. Mater. 27 (2015) 6268–6281, https://doi.org/10.1021/acs.chemmater.5b03156.

[46] D. Villarroel-Rocha, A.A. Godoy, C. Toncón-Leal, J. Villarroel-Rocha, M.S. Moreno, M.C. Bernini, G.E. Narda, K. Sapag, Synthesis of micro–mesoporous CPO-27-Mg@KIT-6 composites and their test in CO_2 adsorption, N. J. Chem. 44 (2020) 10056–10065, https://doi.org/10.1039/C9NJ06358G.

[47] J. Elfving, C. Bajamundi, J. Kauppinen, T. Sainio, Modelling of equilibrium working capacity of PSA, TSA and TVSA processes for CO_2 adsorption under direct air conditions, J. CO_2 Util. 22 (2017) 270–277, https://doi.org/10.1016/j.jcou.2017.10.010.

[48] A. Luukkonen, J. Elfving, E. Inkeri, Improving adsorption-based direct air capture performance through operating parameter optimization, Chem. Eng. J. 471 (2023) 144525, https://doi.org/10.1016/j.cej.2023.144525.

[49] W.R. Lee, S.Y. Hwang, D.W. Ryu, K.S. Lim, S.S. Han, D. Moon, J. Choi, C.S. Hong, Diamine-functionalized metal–organic framework: exceptionally high CO_2 capacities from ambient air and flue gas, ultrafast CO_2 uptake rate, and adsorption mechanism, Energy Environ. Sci. 7 (2014) 744–751, https://doi.org/10.1039/C3EE42328J.

[50] C.J. E. Bajamundi, J. Koponen, V. Ruuskanen, J. Elfving, A. Kosonen, J. Kauppinen, J. Ahola, Capturing CO_2 from air: technical performance and process control improvement, J. CO_2 Util. 30 (2019) 232–239, https://doi.org/10.1016/j.jcou.2019.02.002.

[51] J.A. Wurzbacher, C. Gebald, N. Piatkowski, A. Steinfeld, Concurrent separation of CO_2 and H_2O from air by a temperature-vacuum swing adsorption/desorption cycle, Environ. Sci. Technol. 46 (2012) 9191–9198, https://doi.org/10.1021/es301953k.

[52] W. Li, S. Choi, J.H. Drese, M. Hornbostel, G. Krishnan, P.M. Eisenberger, C. W. Jones, Steam-stripping for regeneration of supported amine-based CO_2 adsorbents, ChemSusChem 3 (2010) 899–903, https://doi.org/10.1002/cssc.201000131.

[53] X. Zhu, T. Ge, F. Yang, R. Wang, Design of steam-assisted temperature vacuum-swing adsorption processes for efficient CO_2 capture from ambient air, Renew. Sust. Energ. Rev. 137 (2021) 110651, https://doi.org/10.1016/j.rser.2020.110651.

[54] V. Stampi-Bombelli, M. van der Spek, M. Mazzotti, Analysis of direct capture of CO_2 from ambient air via steam-assisted temperature–vacuum swing adsorption, Adsorption 26 (2020) 1183–1197, https://doi.org/10.1007/s10450-020-00249-w.

[55] R.P. Wijesiri, G.P. Knowles, H. Yeasmin, A.F.A. Hoadley, A.L. Chaffee, Desorption process for capturing CO_2 from Air with supported amine sorbent, Ind. Eng. Chem. Res. 58 (2019) 15606–15618, https://doi.org/10.1021/acs.iecr.9b03140.

[56] J.M. Kolle, M. Fayaz, A. Sayari, Understanding the effect of water on CO_2 adsorption, Chem. Rev. 121 (2021) 7280–7345, https://doi.org/10.1021/acs.chemrev.0c00762.

[57] C. Gebald, J.A. Wurzbacher, A. Borgschulte, T. Zimmermann, A. Steinfeld, Single-component and binary CO_2 and H_2O adsorption of amine-functionalized cellulose, Environ. Sci. Technol. 48 (2014) 2497–2504, https://doi.org/10.1021/es404430g.

[58] A. Kumar, D.G. Madden, M. Lusi, K. Chen, E.A. Daniels, T. Curtin, J.J. Perry, M. J. Zaworotko, Direct air capture of CO_2 by Physisorbent Materials, Angew. Chem. Int. Ed. 54 (2015) 14372–14377, https://doi.org/10.1002/anie.201506952.

[59] A. Sayari, Y. Belmabkhout, Stabilization of amine-containing CO_2 adsorbents: dramatic effect of water vapor, J. Am. Chem. Soc. 132 (2010) 6312–6314, https://doi.org/10.1021/ja1013773.

[60] M. Yang, C. Ma, M. Xu, S. Wang, L. Xu, Recent advances in CO_2 adsorption from air: a review, Curr. Pollut. Rep. 5 (2019) 272–293, https://doi.org/10.1007/s40726-019-00128-1.

[61] J.A. Mason, T.M. McDonald, T.-H. Bae, J.E. Bachman, K. Sumida, J.J. Dutton, S. S. Kaye, J.R. Long, Application of a high-throughput analyzer in evaluating solid adsorbents for post-combustion carbon capture via multicomponent adsorption of CO_2, N_2, and H_2O, J. Am. Chem. Soc. 137 (2015) 4787–4803, https://doi.org/10.1021/jacs.5b00838.

[62] H. Jo, W.R. Lee, N.W. Kim, H. Jung, K.S. Lim, J.E. Kim, D.W. Kang, H. Lee, V. Hiremath, J.G. Seo, H. Jin, D. Moon, S.S. Han, C.S. Hong, Fine-tuning of the carbon dioxide capture capability of diamine-grafted metal-organic framework adsorbents through amine functionalization, ChemSusChem 10 (2017) 541–550, https://doi.org/10.1002/cssc.201601203.

[63] H.T. Kwon, M.A. Sakwa-Novak, S.H. Pang, A.R. Sujan, E.W. Ping, C.W. Jones, Aminopolymer-impregnated Hierarchical silica structures: unexpected equivalent CO_2 uptake under simulated air capture and flue gas capture conditions, Chem. Mater. 31 (2019) 5229–5237, https://doi.org/10.1021/acs.chemmater.9b01474.

[64] J. Elfving, C. Bajamundi, J. Kauppinen, Characterization and performance of direct air capture sorbent, Energy Procedia 114 (2017) 6087–6101, https://doi.org/10.1016/j.egypro.2017.03.1746.

[65] R. Veneman, N. Frigka, W. Zhao, Z. Li, S. Kersten, W. Brilman, Adsorption of H_2O and CO_2 on supported amine sorbents, Int. J. Greenh. Gas Control 41 (2015) 268–275, https://doi.org/10.1016/j.ijggc.2015.07.014.

[66] A. Sinha, M.J. Realff, A parametric study of the techno-economics of direct CO_2 air capture systems using solid adsorbents, AIChE J. 65 (2019), https://doi.org/10.1002/aic.16607.

[67] S.A. Didas, M.A. Sakwa-Novak, G.S. Foo, C. Sievers, C.W. Jones, Effect of amine surface coverage on the Co-Adsorption of CO_2 and Water: spectral deconvolution of adsorbed species, J. Phys. Chem. Lett. 5 (2014) 4194–4200, https://doi.org/10.1021/jz502032c.

[68] J.S.A. Carneiro, G. Innocenti, H.J. Moon, Y. Guta, L. Proaño, C. Sievers, M. A. Sakwa-Novak, E.W. Ping, C.W. Jones, Insights into the Oxidative degradation mechanism of solid amine sorbents for CO_2 capture from air: roles of atmospheric water, Angew. Chem. Int. Ed. 62 (2023), https://doi.org/10.1002/anie.202302887.

[69] Z. Bacsik, N. Ahlsten, A. Ziadi, G. Zhao, A.E. Garcia-Bennett, B. Martín-Matute, N. Hedin, Mechanisms and kinetics for sorption of CO_2 on bicontinuous mesoporous silica modified with *n*-propylamine, Langmuir 27 (2011) 11118–11128, https://doi.org/10.1021/la202033p.

[70] A.A. Voskanyan, V.G. Goncharov, N. Novendra, X. Guo, A. Navrotsky, Thermodynamics drives the stability of the MOF-74 family in water, ACS Omega 5 (2020) 13158–13163, https://doi.org/10.1021/acsomega.0c01189.

[71] J.M. Veleta, R.A. Arrieta, Y. Wu, M.A. Baeza, K. Castañeda, D. Villagrán, Enhanced gas adsorption on $Cu_3(BTC)_2$ metal–organic framework by post-synthetic cation exchange and computational analysis, Langmuir 39 (2023) 8091–8099, https://doi.org/10.1021/acs.langmuir.3c00455.

[72] A. Justin, J. Espín, I. Kochetygov, M. Asgari, O. Trukhina, W.L. Queen, A Two step postsynthetic modification strategy: appending short chain polyamines to Zn-NH2-BDC MOF for enhanced CO_2 adsorption, Inorg. Chem. 60 (2021) 11720–11729, https://doi.org/10.1021/acs.inorgchem.1c01216.

[73] J.S. Yeon, W.R. Lee, N.W. Kim, H. Jo, H. Lee, J.H. Song, K.S. Lim, D.W. Kang, J. G. Seo, D. Moon, B. Wiers, C.S. Hong, Homodiamine-functionalized metal–organic frameworks with a MOF-74-type extended structure for superior selectivity of CO_2 over N_2, J. Mater. Chem. A 3 (2015) 19177–19185, https://doi.org/10.1039/C5TA02357B.

[74] J.H. Choe, H. Kim, M. Kang, H. Yun, S.Y. Kim, S.M. Lee, C.S. Hong, Functionalization of diamine-appended MOF-based adsorbents by ring opening of epoxide: long-term stability and CO_2 recyclability under humid conditions, J. Am. Chem. Soc. 144 (2022) 10309–10319, https://doi.org/10.1021/jacs.2c01488.

[75] P.J. Milner, J.D. Martell, R.L. Siegelman, D. Gygi, S.C. Weston, J.R. Long, Overcoming double-step CO_2 adsorption and minimizing water co-adsorption in bulky diamine-appended variants of $Mg_2(dobpdc)$, Chem. Sci. 9 (2017) 160–174, https://doi.org/10.1039/c7sc04266c.

[76] M. Jahandar Lashaki, S. Khiavi, A. Sayari, Stability of amine-functionalized CO_2 adsorbents: A multifaceted puzzle, Chem. Soc. Rev. 48 (2019) 3320–3405, https://doi.org/10.1039/c8cs00877a.

[77] A. Sayari, A. Heydari-Gorji, Y. Yang, CO_2-induced degradation of amine-containing adsorbents: reaction products and pathways, J. Am. Chem. Soc. 134 (2012) 13834–13842, https://doi.org/10.1021/ja304888a.

[78] M. Kang, J.E. Kim, D.W. Kang, H.Y. Lee, D. Moon, C.S. Hong, A diamine-grafted metal–organic framework with outstanding CO_2 capture properties and a facile coating approach for imparting exceptional moisture stability, J. Mater. Chem. A 7 (2019) 8177–8183, https://doi.org/10.1039/C8TA07965J.

[79] Y. Seok Chae, S. Park, D. Won Kang, D. Won Kim, M. Kang, D. San Choi, J. Hyeak Choe, C. Seop Hong, Moisture-tolerant diamine-appended metal–organic framework composites for effective indoor CO_2 capture through facile spray coating, Chem. Eng. J. 433 (2022) 133856, https://doi.org/10.1016/j.cej.2021.133856.